4. BASIN MATERIALS–ORIENTALE

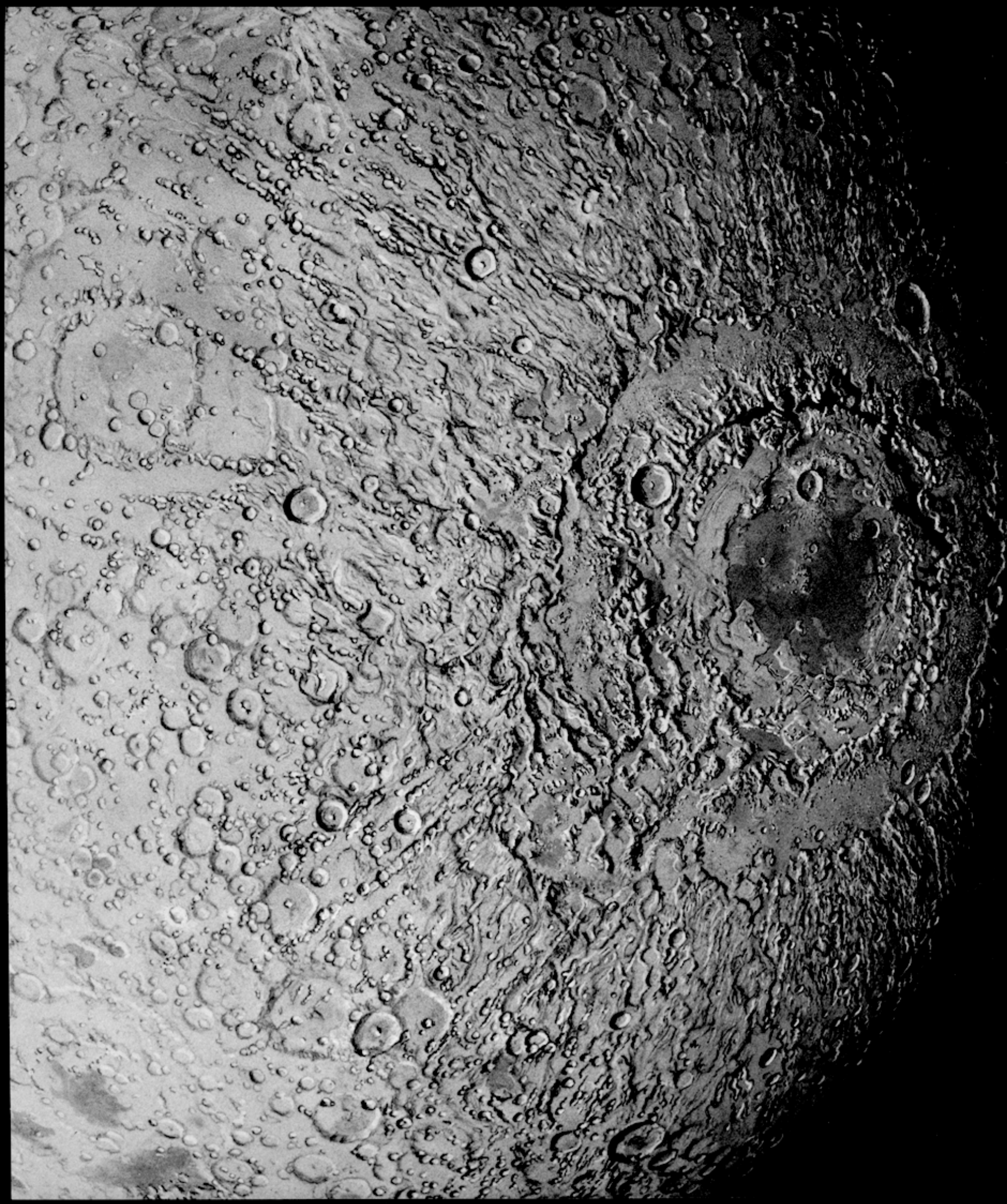

FIGURE 4.1. (OVERLEAF)—Orientale basin and its deposits. Scene centered on farside. Double-ringed basins are Hertzsprung (above) and Apollo (below, with some mare fill). Painting by Donald E. Davis, courtesy of the artist.

4. BASIN MATERIALS—ORIENTALE

CONTENTS

INTRODUCTION

Most simple craters, almost all complex craters, and all ringed basins were formed by impacts. Collectively, these lunar features constitute a series of impact excavations that have many common properties over the entire size range but also show many differences (figs. 4.1–4.3).

Appreciation of the importance to lunar geology of the largest members of this size-morphology series, the basins, has grown slowly. Gilbert (1893) may have been the first to perceive the Imbrium basin as the largest example of the series on the nearside. This interpretation was supported by other influential early workers who increasingly recognized the distinction between basin and mare (Baldwin, 1949, 1963; Kuiper, 1959; Hartmann and Kuiper, 1962; Mason and Hackman, 1962; Shoemaker, 1962a, b; Shoemaker and Hackman, 1962). Shoemaker and Hackman (1962) pointed out the similarity of the Imbrium-basin ejecta to crater ejecta. Several other authors enunciated the differences in style from craters, while affirming a basic similarity of origin, by stressing the linearity of the basin-radial Imbrium sculpture (Baldwin, 1949, chap. 11; 1978) and the concentricity of the ring systems (Baldwin, 1949, p. 37–46; 1963; Hartmann and Kuiper, 1962; Hartmann, 1981). A landmark study of rectified telescopic photographs by Hartmann and Kuiper (1962) documented the ring patterns and regular ring spacings of 12 telescopically visible basins, including Orientale; they also coined the term "basin" (Hartmann and Kuiper, 1962, p. 62; Hartmann and Wood, 1971, p. 3–5; Hartmann, 1981). McCauley (1964b, 1967a, b, 1968) then pointed out similarities of the circum-Orientale terrane to the Imbrium ejecta. Titley and Eggleton (1964; Titley, 1967) tentatively recognized ejecta of the Humorum basin, and Wilhelms and Trask (1965) suggested that the terrane around other basins contains basin ejecta and secondary-impact craters. Stuart-Alexander and Howard (1970) and Hartmann and Wood (1971) reviewed the photographs obtained of the whole Moon in 1966 and 1967 by the five Lunar Orbiters and described the properties, distribution, and probable origins of many additional basins and their maria.

Although these studies established the existence and the impact origin of many large basins, the morphology and extent of the exterior deposits and secondary craters were poorly known before Apollo exploration began (Mutch, 1970; Wilhelms, 1970b). Volcanic and tectonic hypotheses still competed vigorously with impact hypotheses. The first new data that would eventually lead to the current impact model were the superb photographs of the Orientale basin obtained in 1967 by Lunar Orbiter 4 (figs. 1.9, 4.4). The Orientale deposits are less obscured by later material than are those of any other large well-photographed basin. The second and vital clue came from the discovery of complex impact breccia at every sampling site in the terrae, in particular, the Apollo 16 landing site, previously thought to be underlain by volcanic materials (see chap. 2; Howard and others, 1974). The third new development was the extension of impact interpretations to the rest of the terrae, an exercise summarized in this volume. More and more basins have been recognized and established as the sources of surrounding deposits and satellitic craters (pl. 3; fig. 4.3; tables 4.1–4.3).

FIGURE 4.2 (OVERLEAF).—Crater-to-basin transition.

A. Antoniadi (135 km, 70° S., 172° W.), with both an inner ring and a small central peak. Mare material fills depression inside inner ring and partly floods peak. Orbiter 4 frame M–8.

B. Compton (162 km, 56° N., 105° E.), with conspicuous central peak and low but distinct inner "peak ring." Cracks indicate floor uplift. Orbiter 5 frame M–181.

C. Petavius (177 km, 25° S., 60° E.), with massive complex central peak and vague ringlike configuration of low peaks between central peak and wall. Uplift extending to middle of wall is indicated by grabens. Slight filling by dark material is evident along walls. Orbiter 4 frame H–184.

D. Gauss (177 km, 36° N., 79° E.), with entirely different floor structure from that of Petavius, although both craters are of same size. Orbiter 4 frame H–165.

E. Humboldt (207 km, 27° S., 81° E.), with central peak and line of peaks. Other rugged features of original floor are higher in north than in south; cracks indicate uplift of entire floor. Light-colored plains may be later fill; dark crescents are later mare fill. Orbiter 4 frame M–12.

F. Landau (221 km, 43° N., 119° W.), with few distinct floor features; irregularly depressed in northeast. Orbiter 5 frame M–12.

G. Campbell (225 km, 45° N., 153° E.), with some offcenter rugged relief. An offcenter depression, as in Landau, is here filled by a small mare patch. Orbiter 5 frame M–103 (rectified).

H. Clavius (225 km, 58° S., 14° W.), with small offcenter peaks, probably partly covered by later plains fill. Orbiter 4 frame M–124.

I. Schwarzschild (235 km, 71° N., 120° E.), with rugged, arcuate, crescent-shaped floor topography. Orbiter 4 frame M–92.

J. Milne (262 km, 32° S., 113° E.), with complex single to triple arcs. Milne and Schwarzschild are the most basinlike craters smaller than 300 km in diameter. Orbiter 3 frame M–121.

K. Gagarin (272 km, 20° S., 149° E.), with indistinct ring-form structure, though larger than Milne. Orbiter 1 frame M–116.

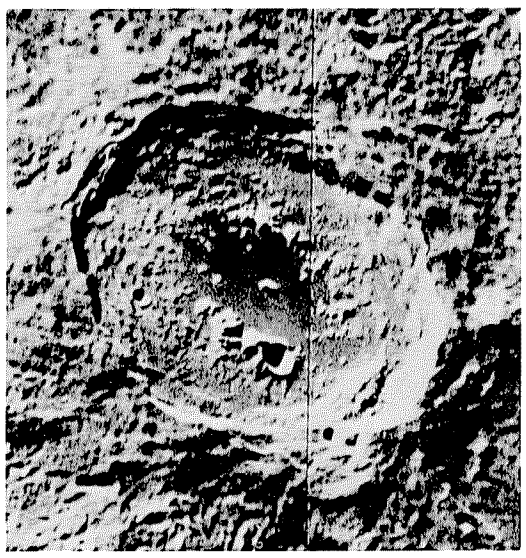

A

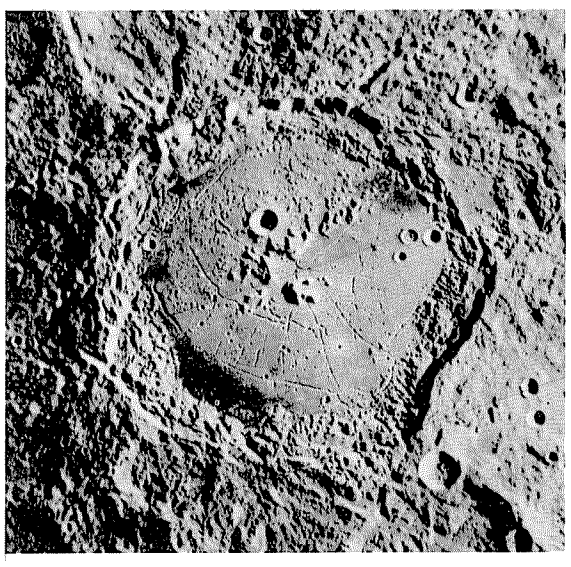

E

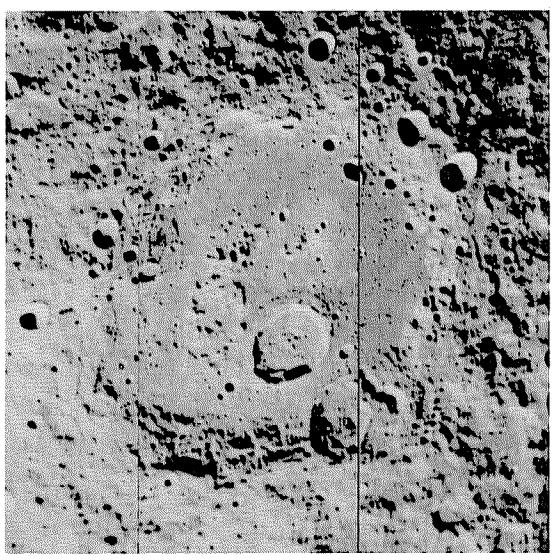

I

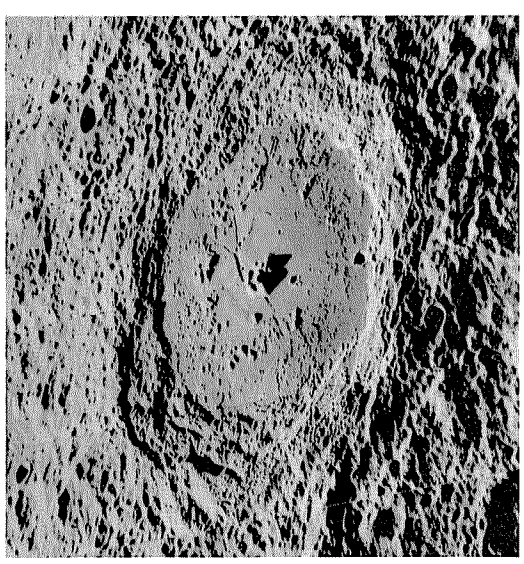

B

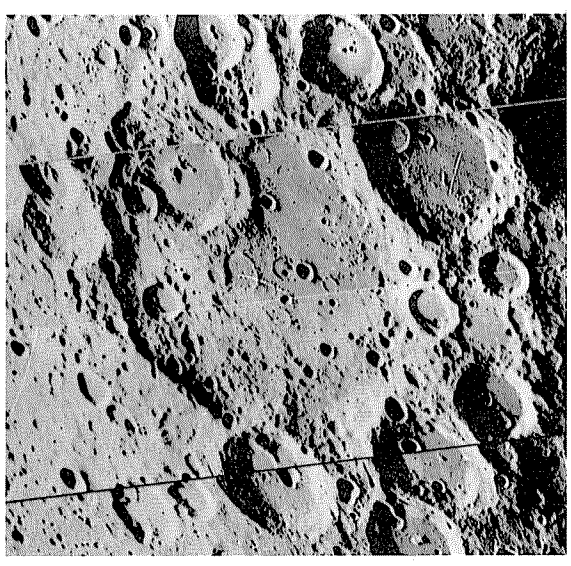

F

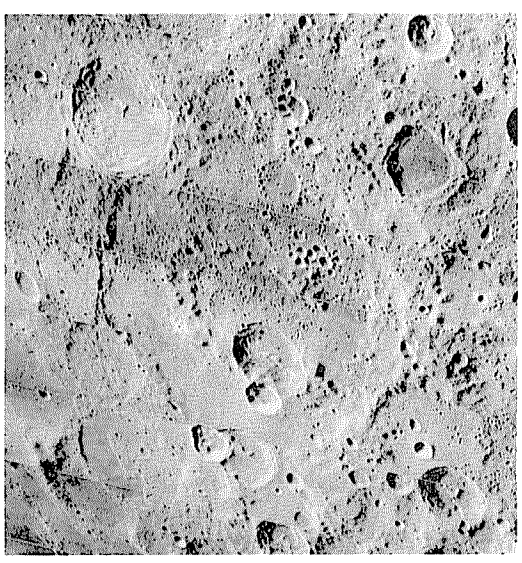

J

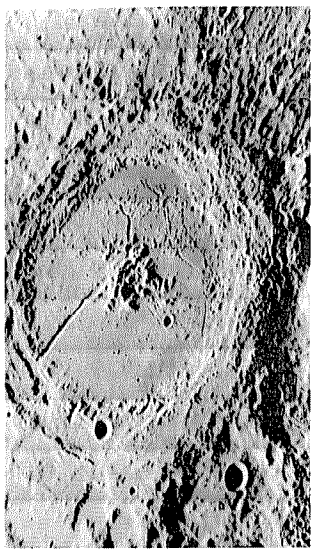

C

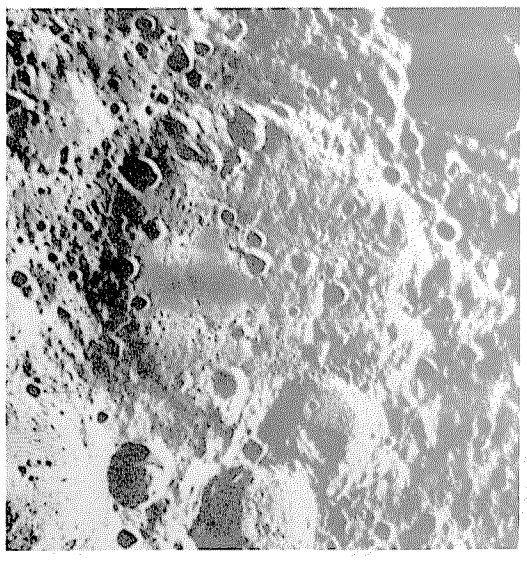

G

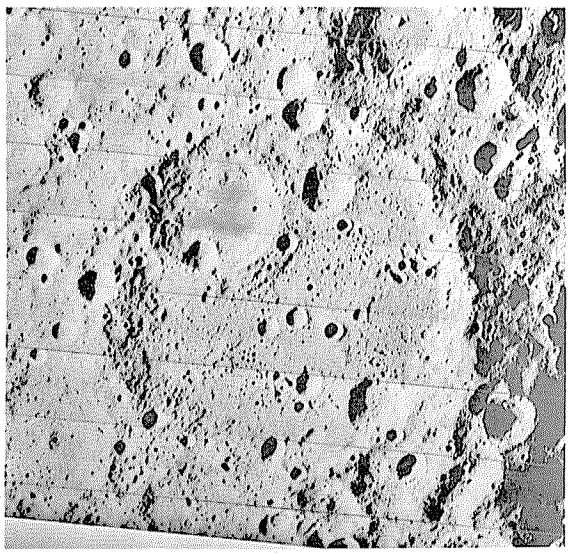

K

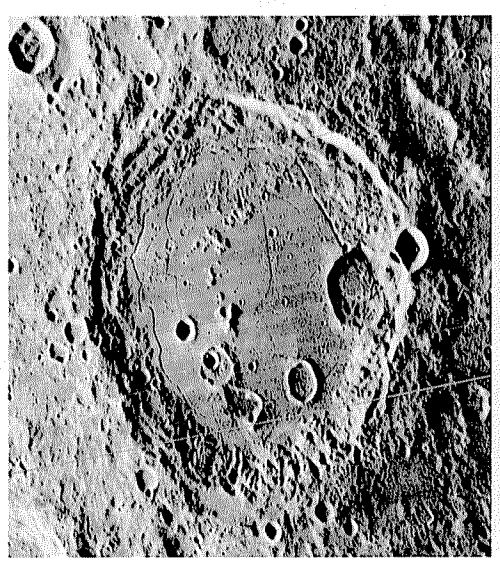

D

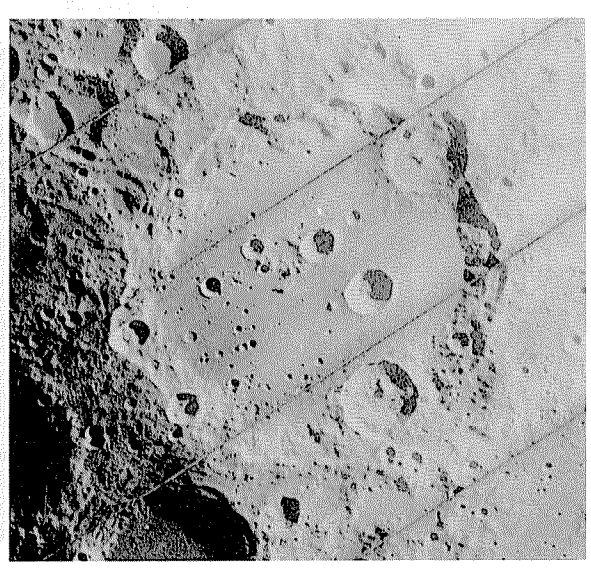

H

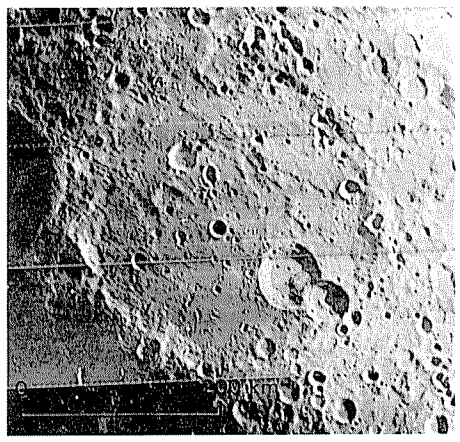

A. Bailly.

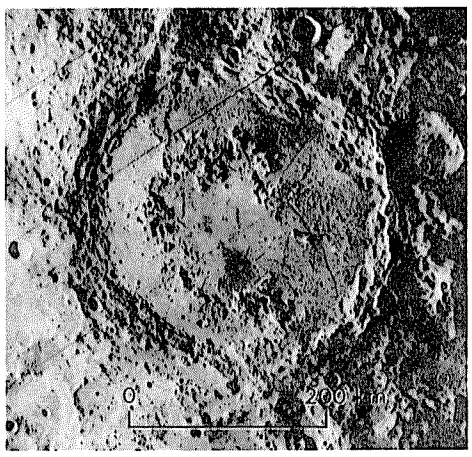

B. Schrödinger.

C. Schiller-Zucchius.

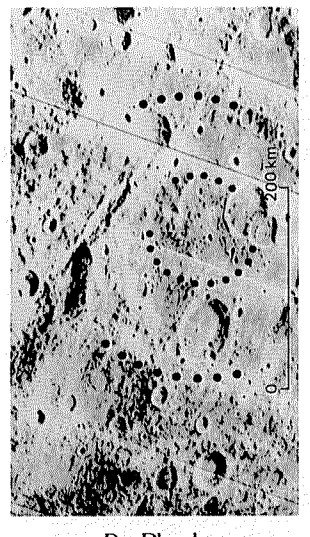

D. Planck.

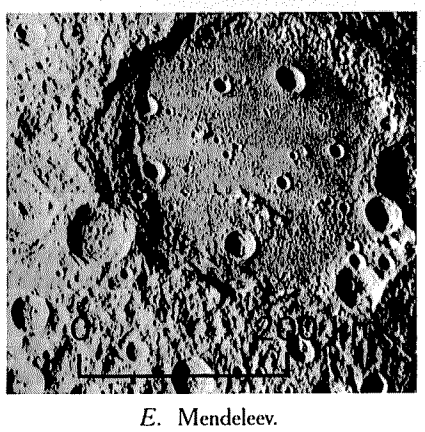

E. Mendeleev.

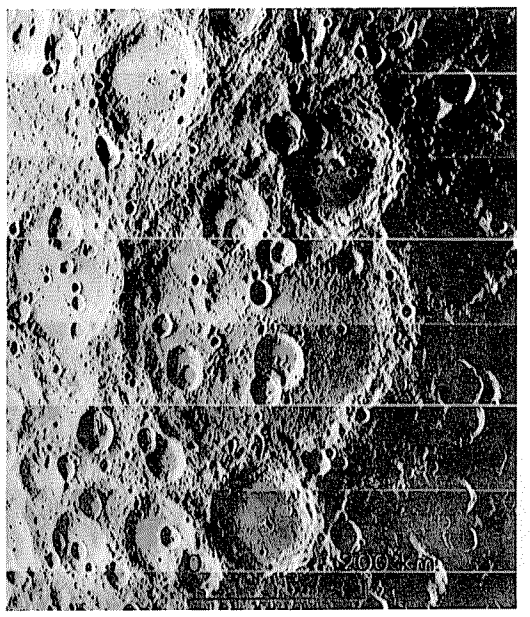

F. Birkhoff.

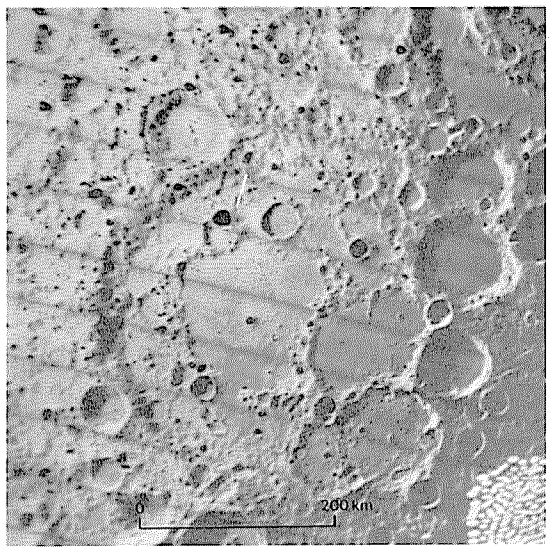

G. Poincaré.

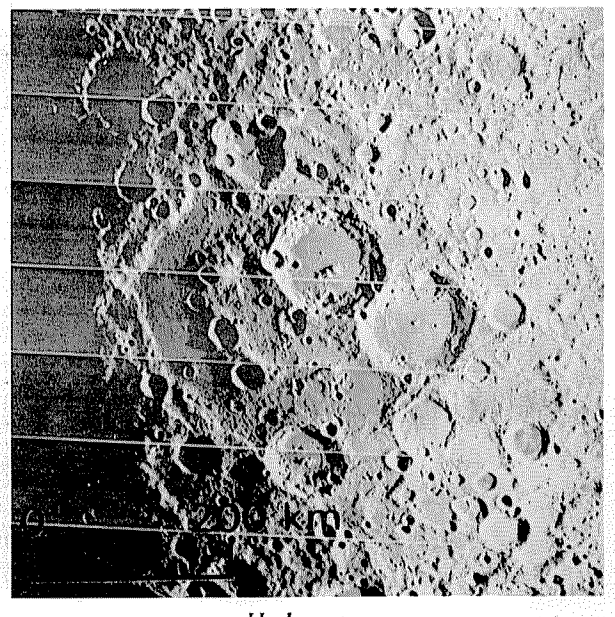

H. Lorentz.

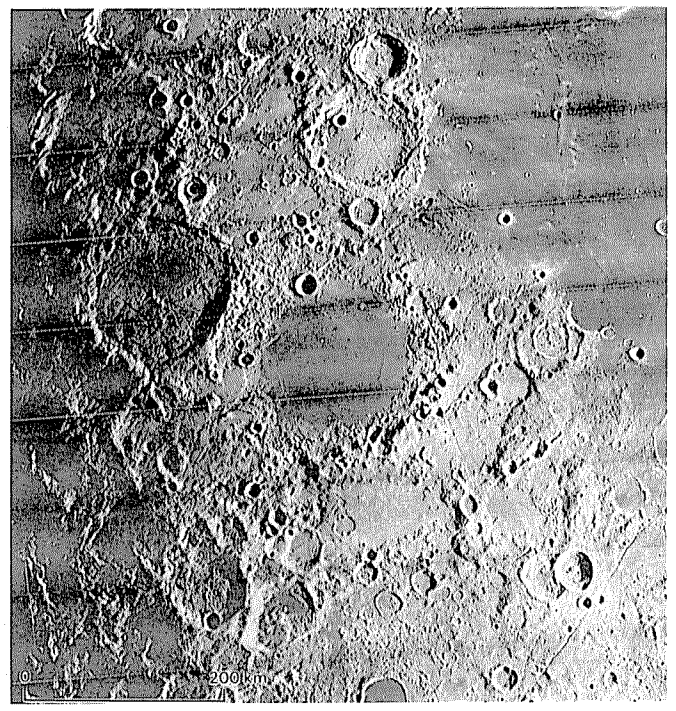

I. Grimaldi.

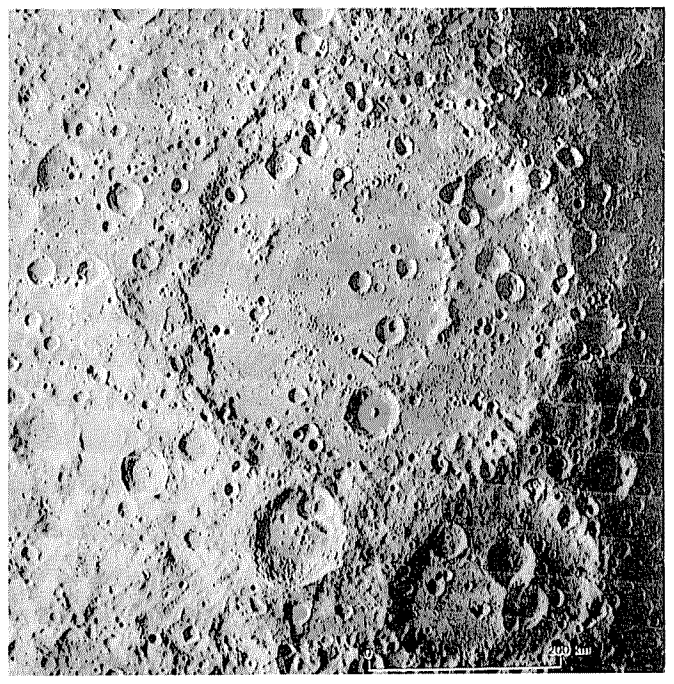

J. Korolev.

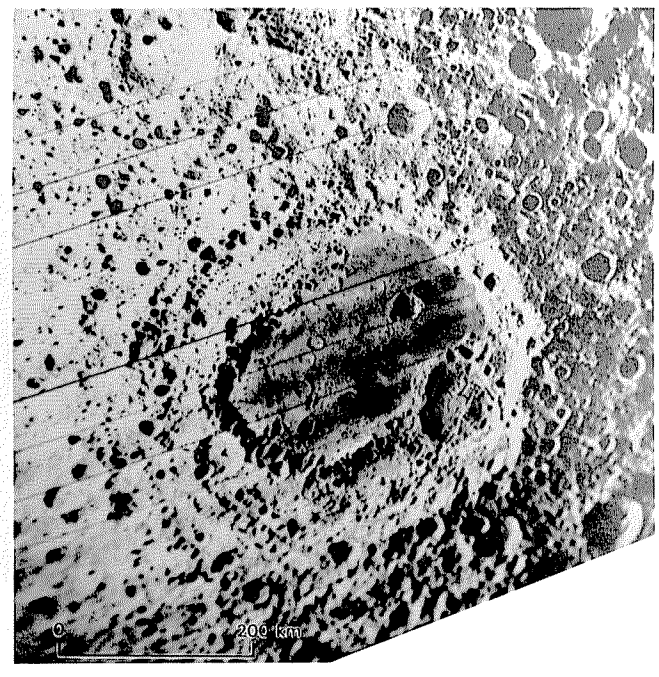

K. Moscoviense.

FIGURE 4.3.—Definite lunar basins at least 300 km in diameter, in order of increasing size and complexity (see table 4.1).

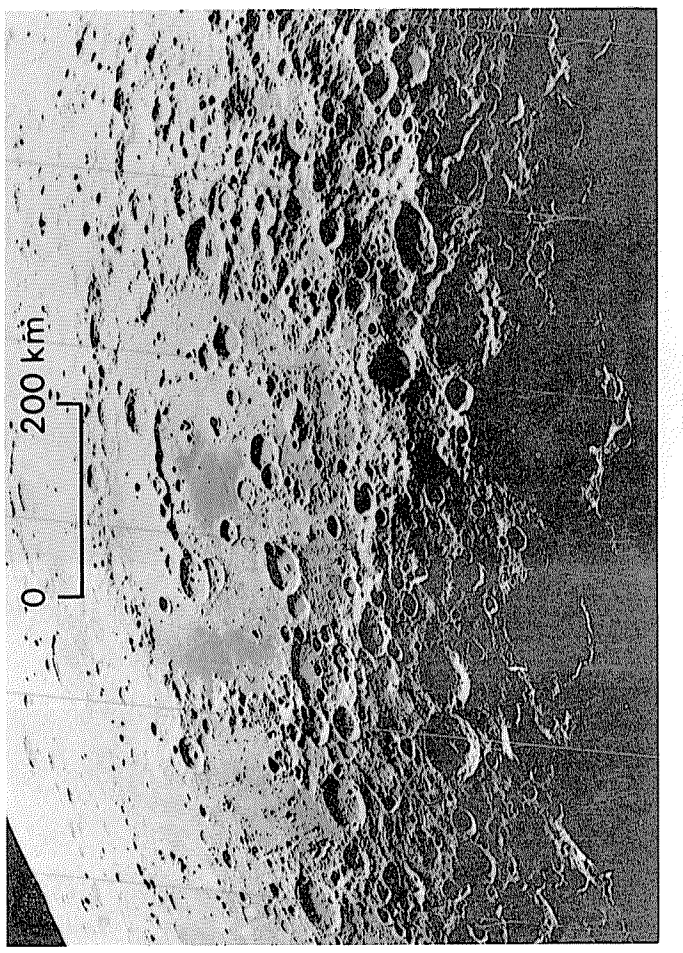

L. Apollo.

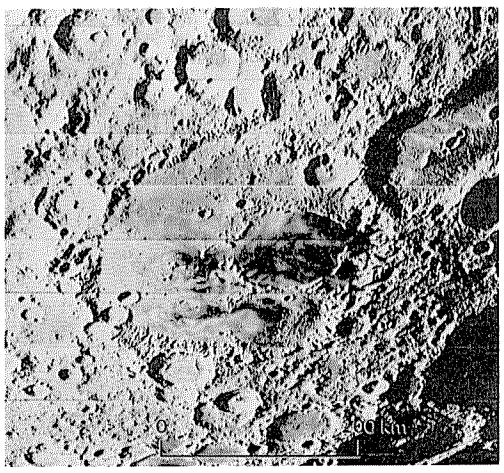

N. Ingenii.

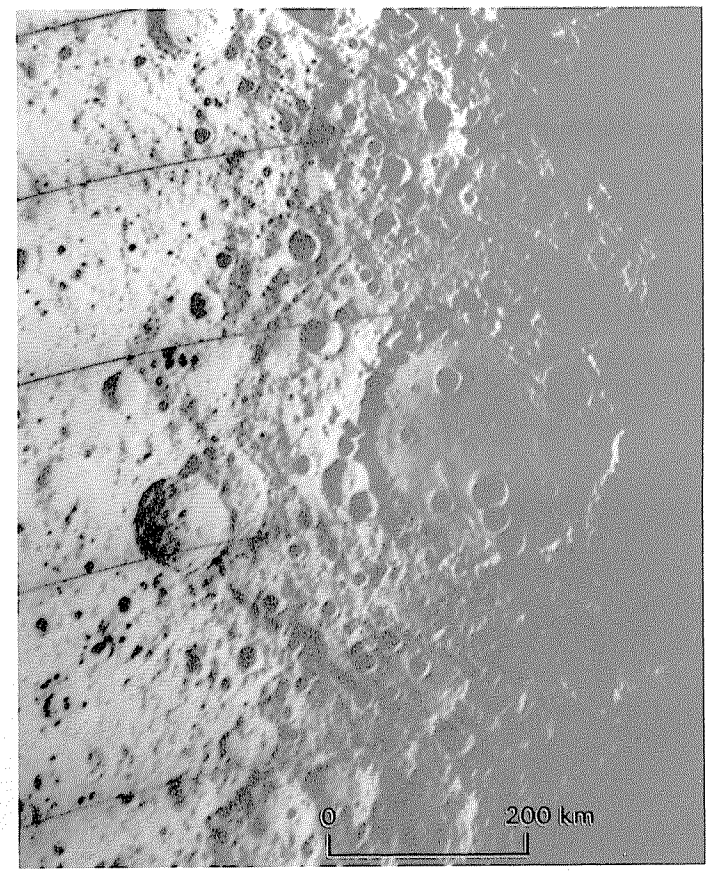

O. Hertzsprung.

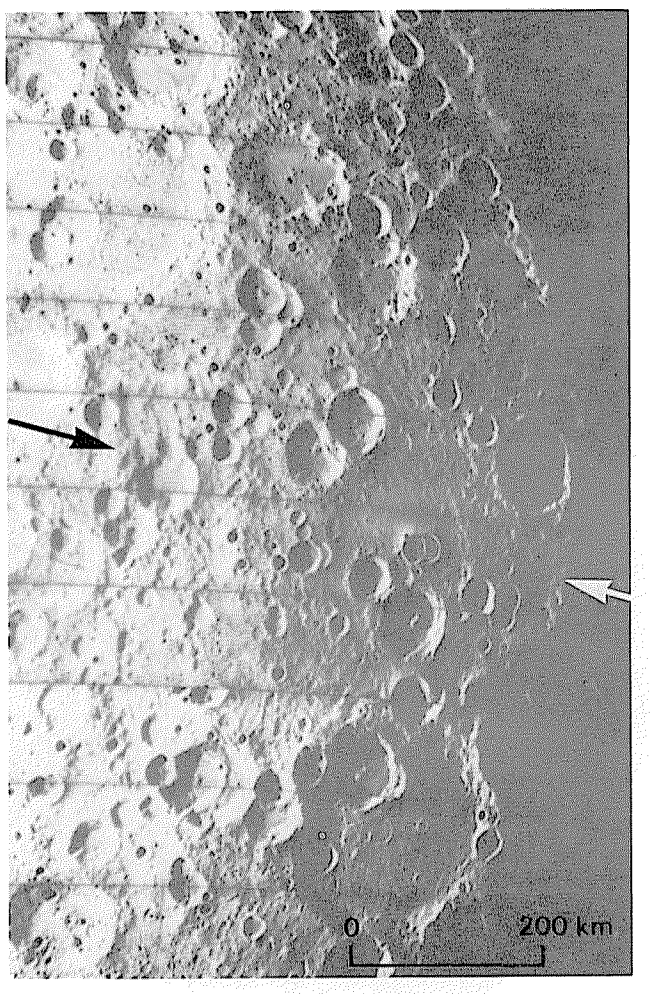

M. Coulomb-Sarton.

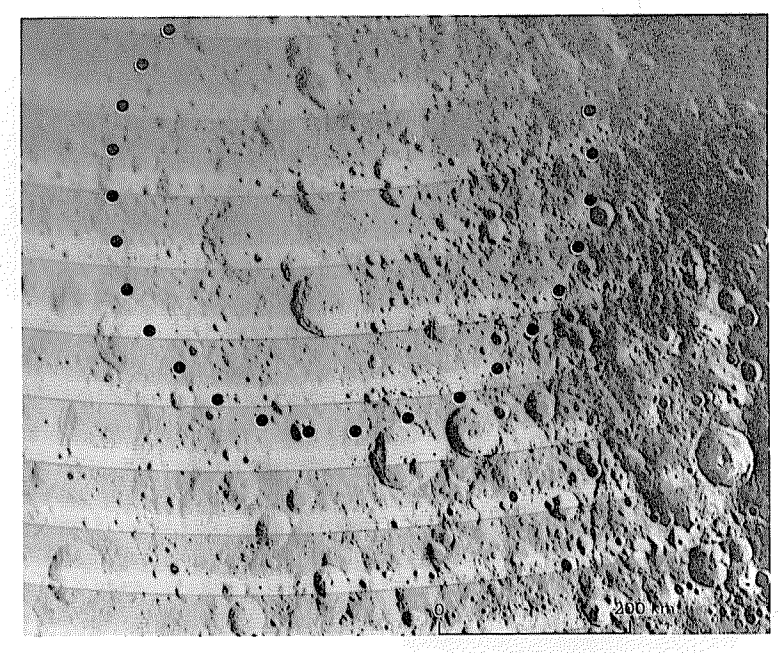

P. Freundlich-Sharonov.

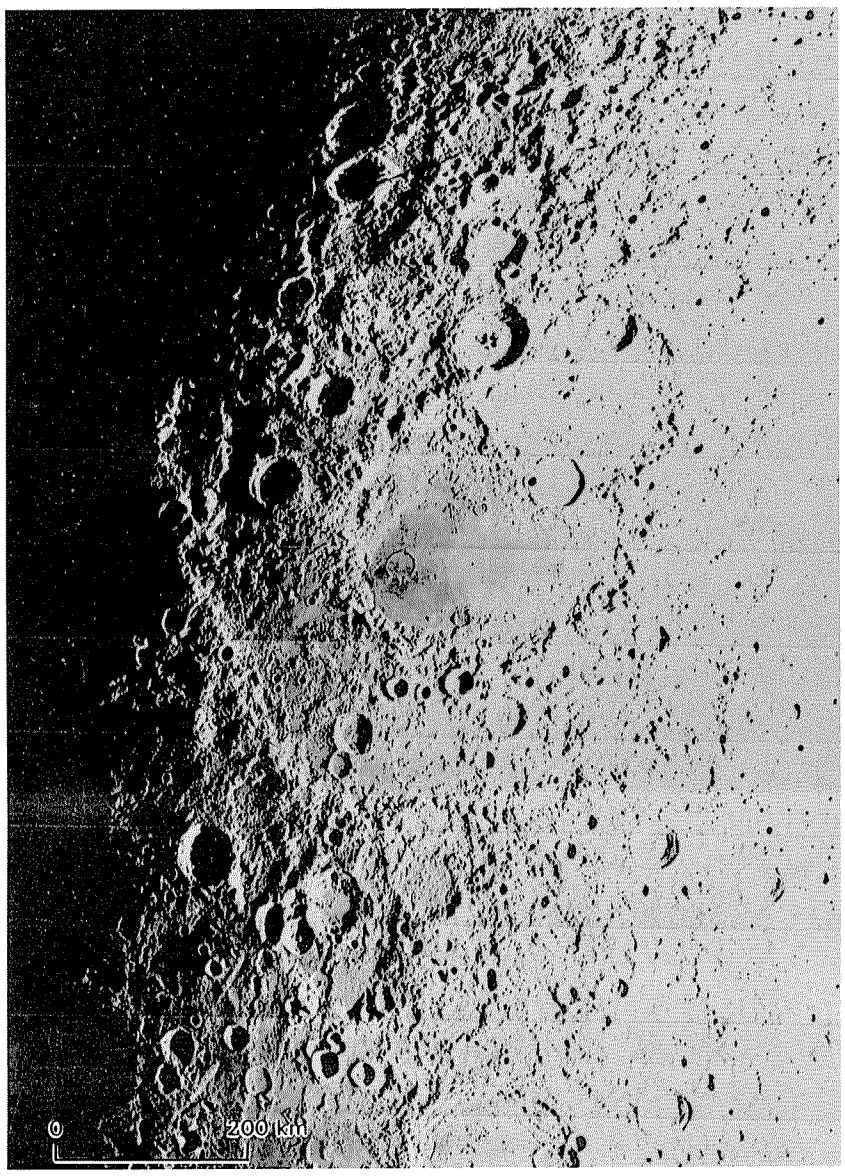

Q. Humboldtianum.

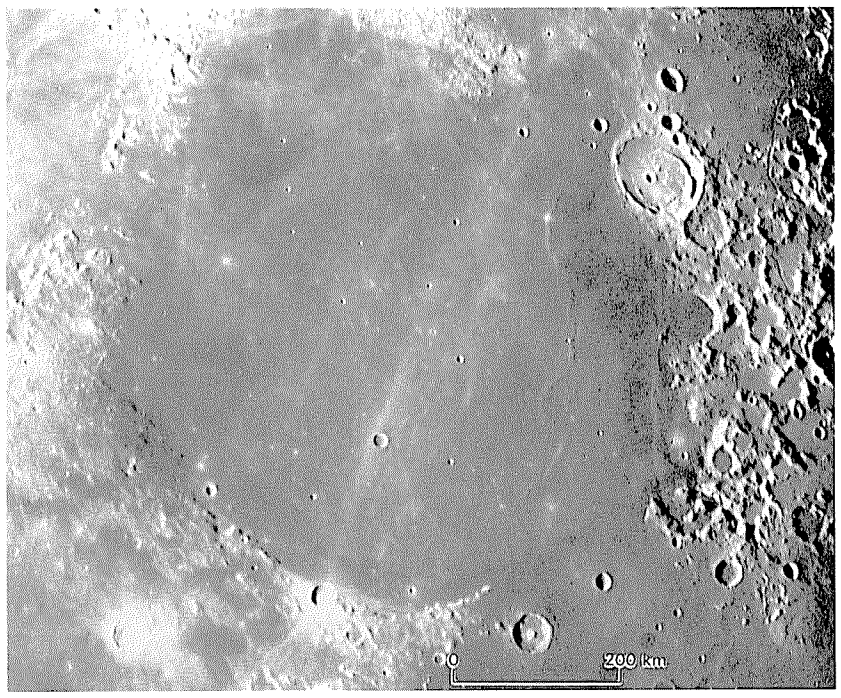

S. Serenitatis.

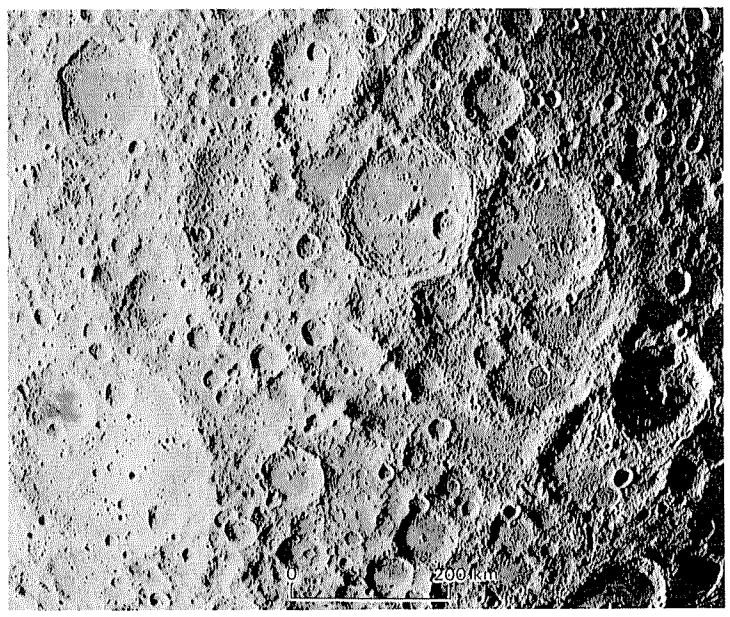

T. Keeler-Heaviside.

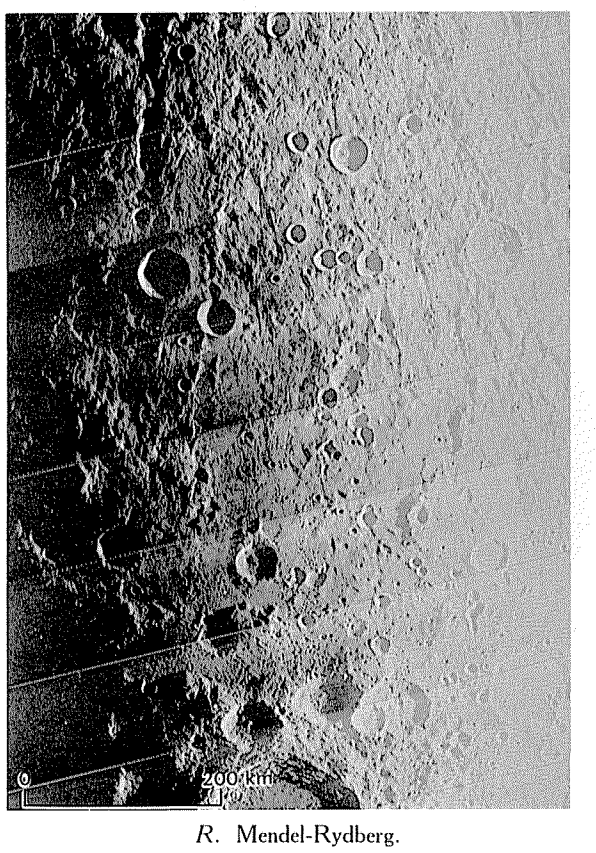

R. Mendel-Rydberg.

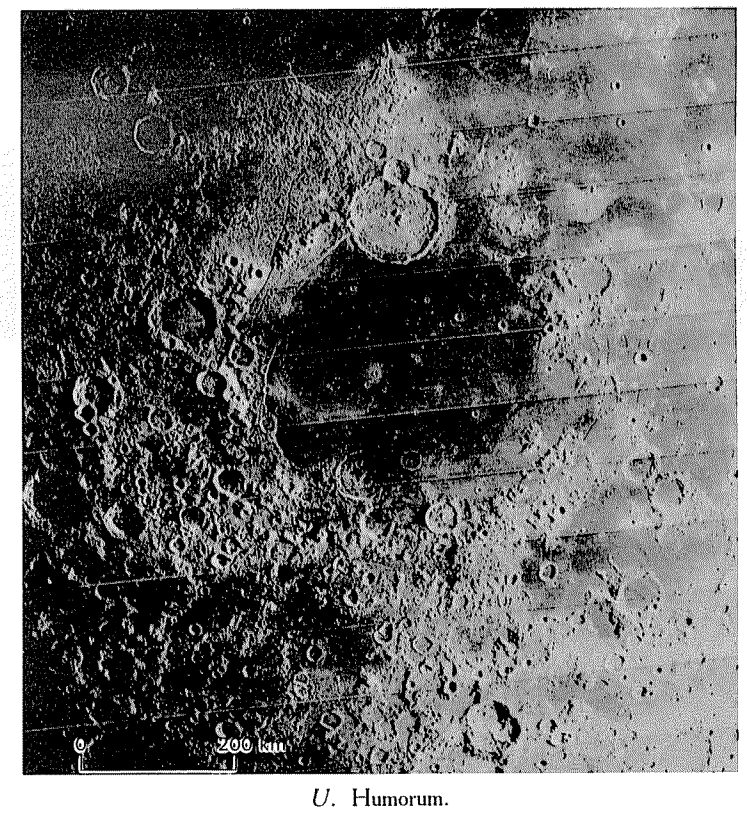

U. Humorum.

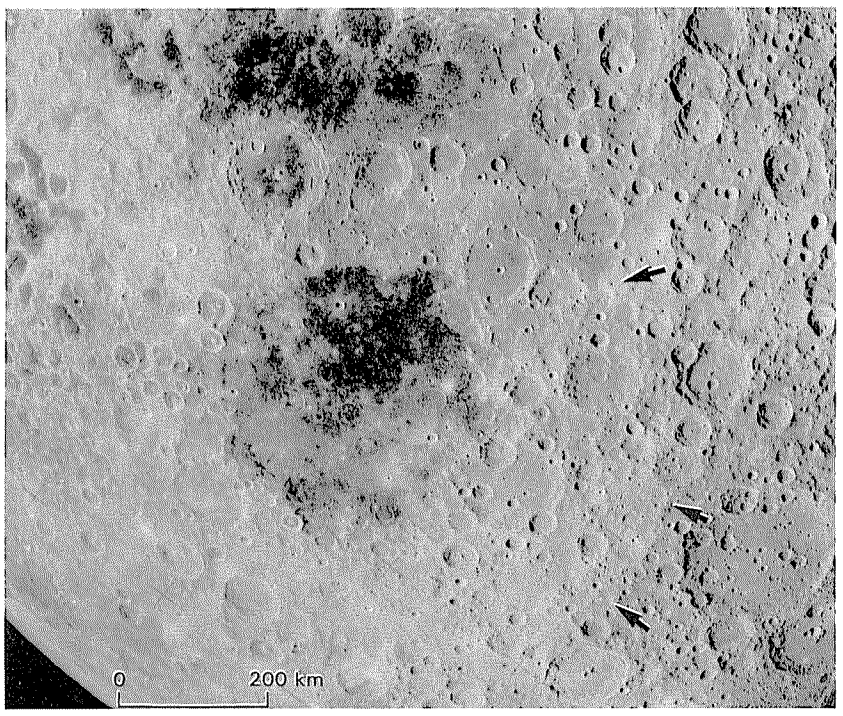

V. Smythii.

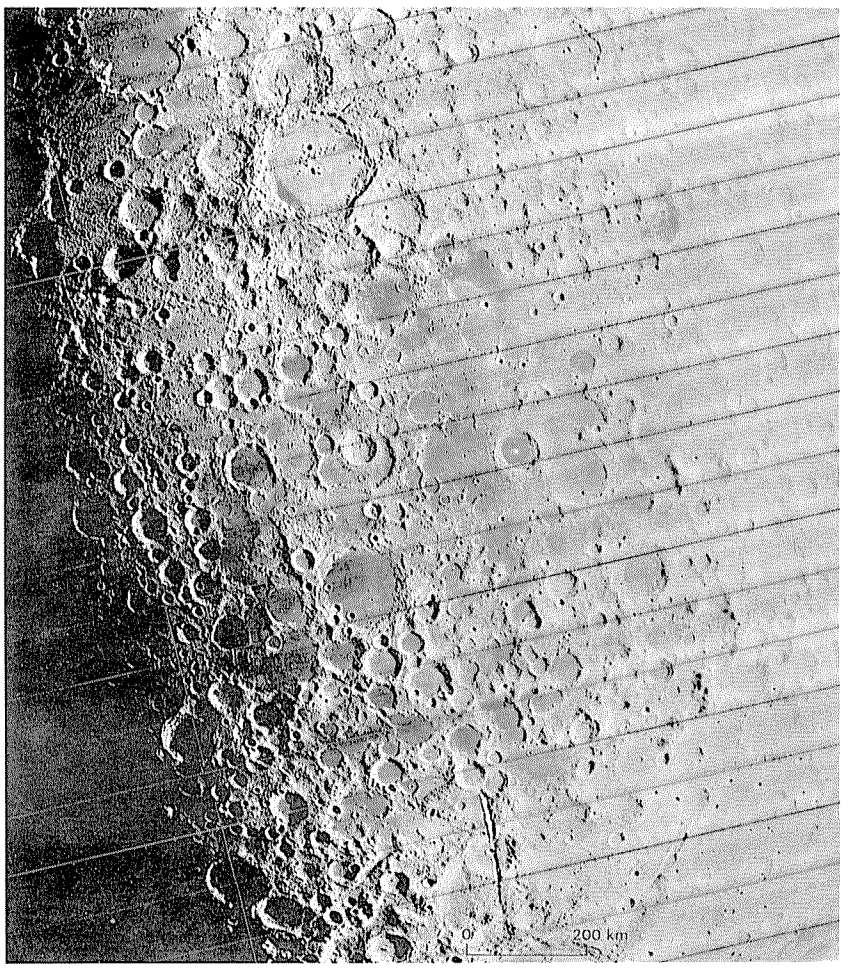

X. Australe.

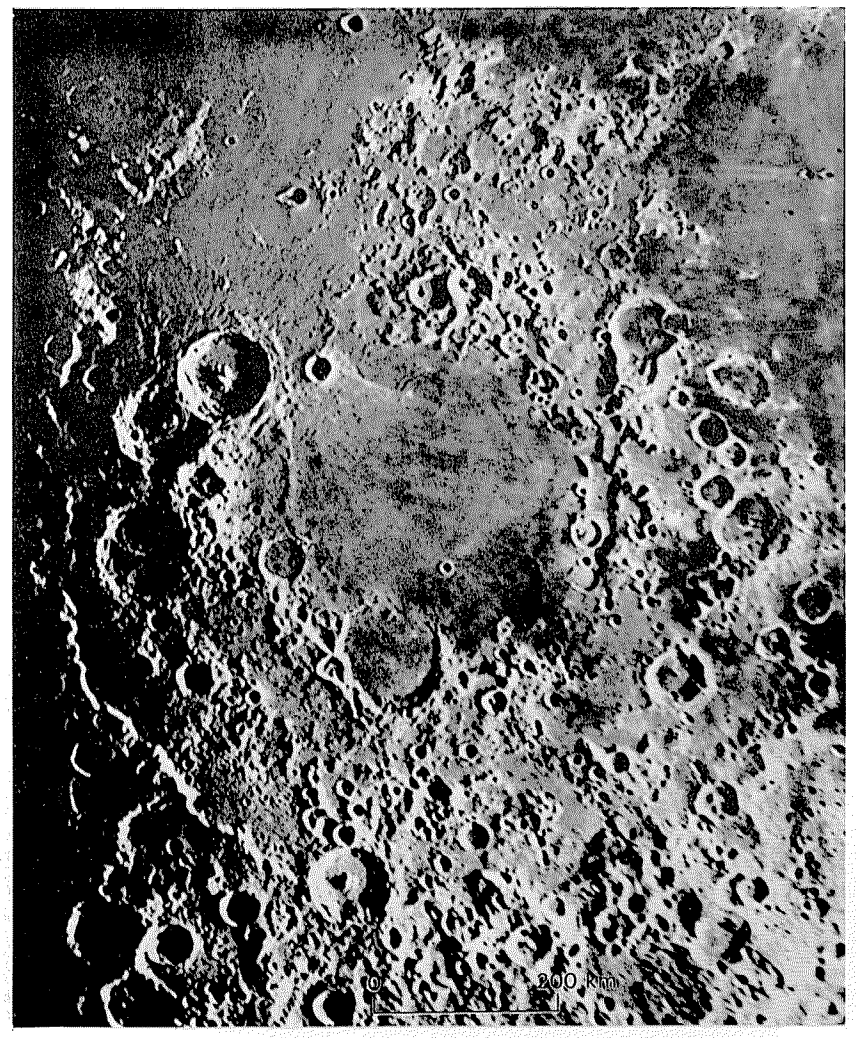

W. Nectaris.

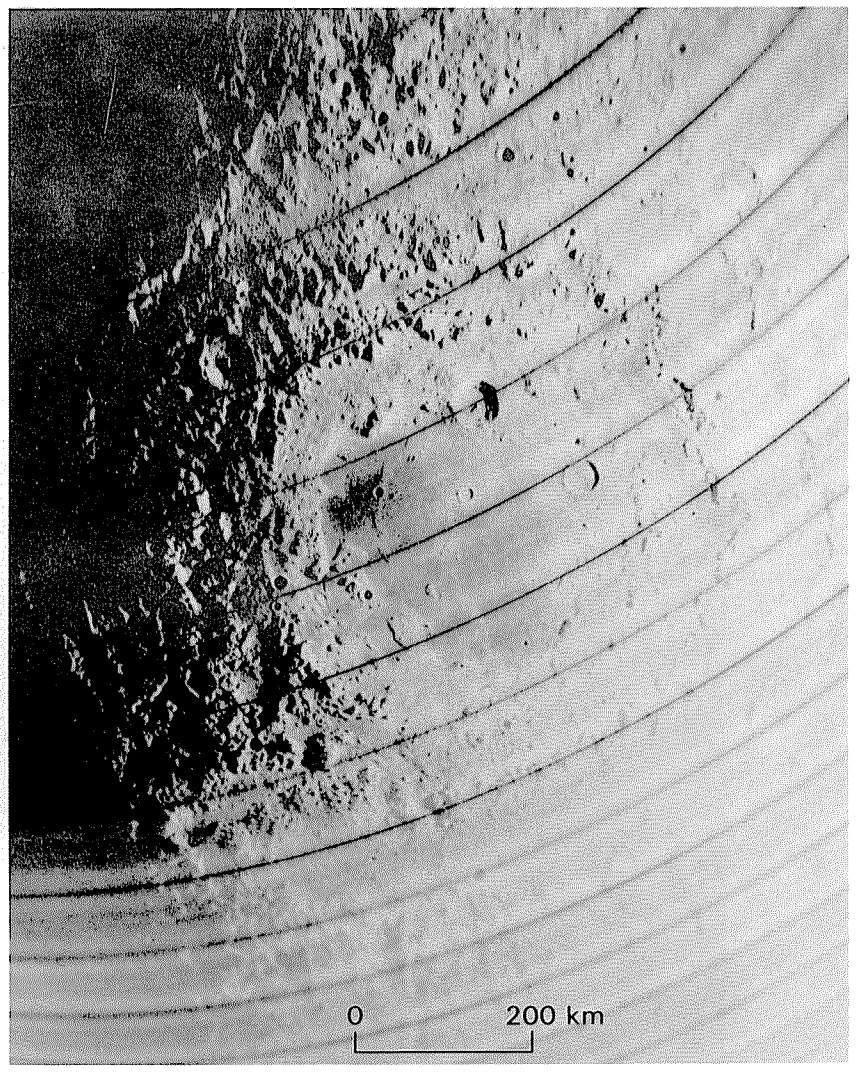

Y. Orientale.

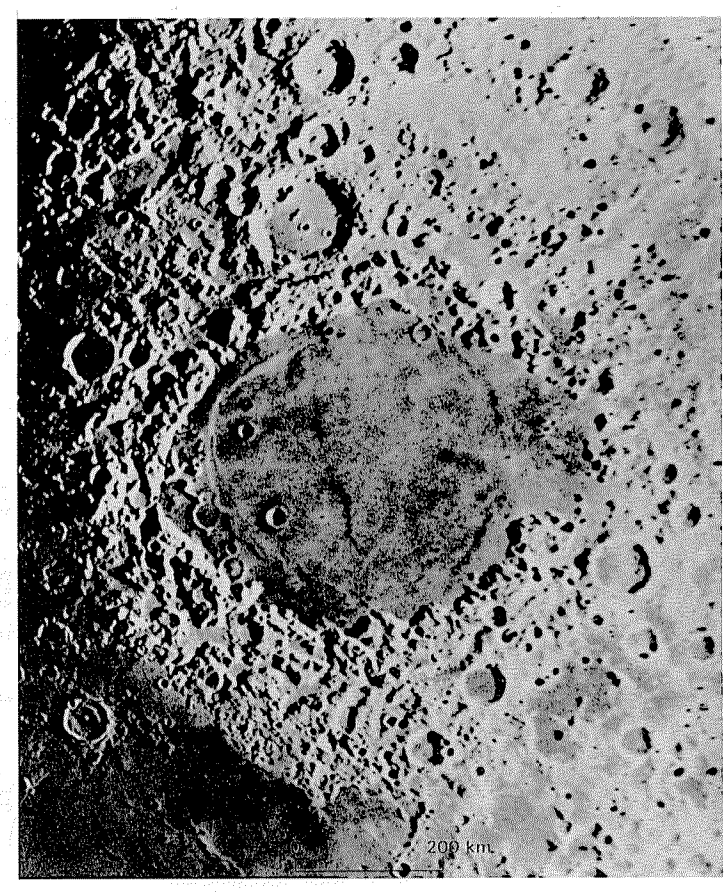

Z. Crisium.

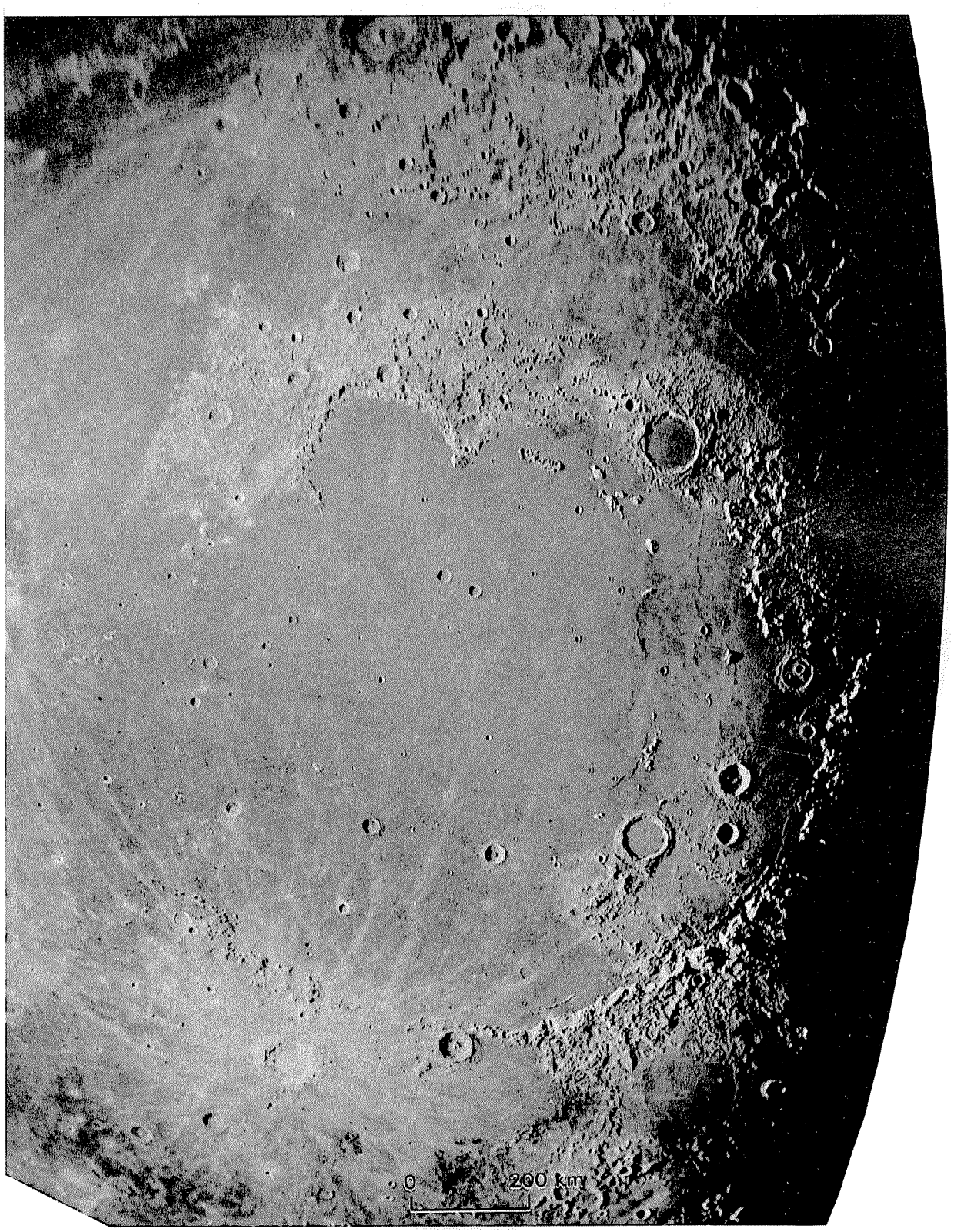

AA. Imbrium.

TABLE 4.1.—*Definite lunar basins at least 300 km in diameter*

[Basins listed in order of increasing size and complexity. Names all in capitals have deposits mapped on plate 3. Names are derived, where possible, either from the mare fill of a basin (for example, the Imbrium basin from Mare Imbrium) or from a name given by the International Astronomical Union, considering them as craters (for example, Apollo). Otherwise, they are named here from two superposed, unrelated craters:

Name used here (reference)	Earlier designation (reference)
Schiller-Zucchius (W79)	Basin near Schiller (HK62).
Coulomb-Sarton (L78)	Unnamed basin B (HW71).
Freundlich-Sharonov (S78)	
Mendel-Rydberg (W79)	SE. limb basin (HK62).
Keeler-Heaviside (S78)	
South Pole-Aitken (S78)	Big backside basin (common usage).

Best photographs: Photograph used in figure 4.3 is underlined; each includes one-half basin radius beyond topographic rim, where possible. HK62, telescopic photograph from Hartmann and Kuiper (1962); r, rectified; A16, Apollo 16 frame; M10, Mariner 10 frame (Mercury-Venus mission that photographed the Moon during flyby). Others are Lunar Orbiter frames.
Major rings: Diameters are listed for rings that are observed or inferred to extend more than half a basin circumference. Approximate radii are listed for partial segments that may not form complete rings. Additional small segments are plotted on plate 3. Topographic basin rim (also called main rim in descriptions) is underlined, queried where uncertain.
References: B49, Baldwin (1949); B63, Baldwin (1963); G93, Gilbert (1893); HK62, Hartmann and Kuiper (1962); HW71, Hartmann and Wood (1971); L78, Lucchitta (1978); M67, McCauley (1967a, b); S77, Scott and others (1977); S78, Stuart-Alexander (1978); SH62, Shoemaker and Hackman (1962); SH70, Stuart-Alexander and Howard (1970); T67, Titley (1967); WE77, Wilhelms and El-Baz (1977); WM71, Wilhelms and McCauley (1971); W79, Wilhelms and others (1979). Chapter numbers refer to the present volume.]

Basin	Figure	Center (lat, long)	Best photographs	Major rings: Diameter (km)	Major rings: Radius (km)	Description	References
Bailly	4.3A	67° S., 68° W.	4 H-179 4 M-193 4 M-179	300 150	--- ---	Degraded craterlike rim. Discontinuous inner ring, connected to rim by outward-sloping shelf. Deposits obscured by Orientale.	Chapter 9; HW71, W79.
SCHRÖDINGER	4.3B	75° S., 134° E.	5 H-21 4 M-8 4 M-94	320 155	--- ---	Fresh craterlike rim and wall. Inner ring consists of rugged crags forming nearly complete circle, joined to wall in two places by exposed shelf. Hummocky probable impact impact melt on floor. Extensive craterlike deposits, linear secondary chains.	Chapter 10; H70, HW71, W79.
Schiller-Zucchius	4.3C	56° S., 44.5° W.	4 H-160 4 M-148 4 M-136	325 165	--- ---	Outer ring craterlike though degraded; bounded inward by steep scarp, outward by gentle flank. Inner ring mountainous. No discernible deposits.	Chapter 8; HK62, W79.
Planck	4.3D	57.5° S., 135.5° E.	3 M-121 4 M-8 4 M-9 4 M-82 5 M-65	325 175	--- ---	Poorly photographed; outer ring apparently craterlike, inner ring partial. No discernible deposits.	Chapter 8; HW71, W79.
MENDELEEV	4.3E	6° N., 141° E.	1 M-115 1 M-136	330 140	--- ---	Craterlike outer rim with flat-bottomed troughs. Inner ring of discontinuous small peaks, connected to wall by outward-sloping shelf. Craterlike deposits and numerous, though subdued, secondary craters.	Chapter 9; WE77, S78.
BIRKHOFF	4.3F	59° N., 147° W.	5 M-29 5 M-29 5 M-25	330 150	--- ---	Craterlike rim. Discontinuous, mostly obscured inner ring of narrow ridges. Extensive craterlike deposits and secondaries.	Chapter 8; HW71, L78.
Poincaré	4.3G	57.5° S., 162° E.	5 M-65(r) 2 M-75 3-M-121 4-M-82	340 175	--- ---	Apparently craterlike rim. Continuous but battered lower inner ring. No deposits observed.	Chapter 8; HW71, W79.
LORENTZ	4.3H	34° N., 97° W.	4 M-189	360 185	--- ---	Craterlike rim. Low and ridgelike inner ring, continuous except where cratered. Craterlike deposits and secondary craters west of basin.	Chapter 8; HW71.
Grimaldi	4.3I	5° S., 68° W.	4 H-163 4 M-161	430 230	--- ---	Obscured by Orientale; probably craterlike rim. Discontinuous rugged inner ring. No deposits observed.	Chapter 8; HK62, WM71.
KOROLEV	4.3J	4.5° S., 157° W.	1 M-38 1 M-28	440 220	--- ---	Craterlike rim locally divided by terracing. Inner ring partly buried but detectable for almost a complete circle. Deposits well exposed to west; extensive secondaries.	Chapter 9; HW71, S78.
MOSCOVIENSE	4.3K	26° N., 147° E.	5 M-103(r) 5 M-124	--- 445 210	275 --- ---	Crude figure-8 pattern of outer and inner rings. Rim has crude echelon pattern suggestive of large-scale terracing. Inner ring complete for half of periphery; has steep inner scarp and broad, gentle outer flank. Deposits and secondaries poorly photographed but visibly reduce prebasin crater population 400 to 500 km from rim.	Chapter 9; HW71, S78.
APOLLO	4.3L	36° S., 151° W.	5 H-30 5 M-30	505 250	--- ---	Interrupted obscured main rim. Bifurcations indicate terracing. Inner ring partly continuous and bounded by steep inward scarp and gentler outer flank, partly discontinuous and rugged. Concavity or discontinuity inside inner ring indicated by mare localization. Mare patches indicate outward slope of interring shelf and possible exterior rings. Deposits and secondaries extend about 500 km southward.	Chapter 8; SH70, HW71, S78.
Coulomb-Sarton	4.3M	62° N., 123° W.	5 M-5 5 M-25(r)	530(?) 400 190	--- --- ---	Heavily obscured by Birkhoff and Lorentz deposits. Rings uncertain; 400-km-diameter ring could be the rim.	Chapter 8; HW71, L78.
Ingenii	4.3N	34° S., 163° E.	2 M-75	560(?) 325	--- ---	Outer ring questionable; consists of discontinuous but large massifs. Inner, 325-km-diameter, mare-bounding ring, more complete, though battered, may be the main rim. Deposits not directly observed but may breach south rim of Keeler-Heaviside basin.	Chapter 8; S78.
HERTZSPRUNG	4.3O	1.5° N., 128.5° W.	5 H-26 5 H-28 5 M-26 5 M-28(r) 5 M-24	570 --- 265 140	--- 205 --- ---	Craterlike rim in most sectors, irregular in northwest and indistinct in north. Half of complete and distinct innermost ring resembles crater rim; rest consists of rugged peaks. Intermediate rings conspicuous, single, and benchlike or ridgelike in most sectors; ragged, bifurcated, echelon in northwest; inconspicuous in north, where ragged ridges and hills form upland nearly at level of surrounding terrain. Deposits extensive, locally 600 km from rim; some secondary-crater lobes 900 km from rim.	Chapter 9; SH70, HW71.
FREUNDLICH-SHARONOV	4.3P	18.5° N., 175° E.	2 M-34(r) 5 M-79	600 ? ?	--- ? ?	Rim complete; seems craterlike but is poorly photographed. Ridges suggest interior ring structure, but connection into rings or terraces is uncertain. Distinct radial grooves and ridges and mantling of craters south of basin indicate deposits and secondaries extending at least 600 km from rim.	Chapter 8; S78.
HUMBOLDTIANUM	4.3Q	61° N., 84° E.	4 H-165 4 M-23 4 M-164 4 M-152 4 M-165 M10 2277	--- 600 275	600 --- ---	Figure-8 shape; each part of main rim about 600 km in diameter, equivalent in total area to a circle 700 km in diameter. Bel'kovich (200 km diam) is either an independent crater or third part of inner basin. Intermediate ring, fairly distinct in south-southwest, consists of hills in southwest, many large hills in southeast, and nearly continuous hilly area in north about at level of surrounding terrain. External 600-km-radius arcs southwest of main rim. Distinct deposits and secondary craters (<20 km diam) extend more than 600 km from southeast rim.	Chapter 9; HK62, L78.
MENDEL-RYDBERG	4.3R	50° S., 94° W.	4 H-193 4 M-193 4 M-186	630(?) 460 --- 200	--- --- 155 ---	Distinct separation of rings in south, but continuity uncertain. Faint deposits in southwest.	Chapter 9; HK62, HW71, W79.
SERENITATIS	4.3S	27° N., 19° E.	Telescopic 4 M-97	--- 740 420	450 --- ---	Ring structure indistinct in west half except in Montes Haemus. Haemus, Taurus-Littrow massifs, and other margins of mare probably form main rim (Head, 1979b). "Vitruvius front" (Head, 1974b) and other irregular elevations form long arcs with 450-km radii. Mare ridges suggest a buried 420-km-diameter ring. Basin may be double, with small northern and large southern components (Scott, 1972a; Wolfe and Reed, 1976); center as listed is that of combined components.	Chapter 9; B49.
Keeler-Heaviside	4.3T	10° S., 162° E.	2 M-75	780(?) --- ---	--- 270 170	All rings and arcs composed of large but disconnected massifs whose connection as rings and relation to excavation boundary are uncertain. Deposits not observed.	Chapter 8; S78.
HUMORUM	4.3U	24° S., 39.5° W.	4 M-143 4 H-136 4 M-136	--- 820(?) --- --- 440 325	? --- 350 280 --- ---	820-km-diameter ring defined by steep notched scarp in south and by discontinuous lower ragged, semiradial or semiconcentric ridges or massifs elsewhere. Part of most conspicuous mare-bounding ring (440 km diam) connects with 280-km-radius arcs as sloping flank, elsewhere is divided into semidistinct rings with bridges to 820-km-diameter ring. 325-km-diameter ring marked by terra shelf and mare bench. Most distinct ring separation is in south. Deposits and secondary craters distinct only in southeast.	Chapter 9; HK62, T67, WM71.
Smythii	4.3V	2° S., 87° E.	4 M-9,11 2 M-196 A16 M-3035 4 M-17	--- 840 --- 360	480 --- 330 ---	840-km-diameter ring defined by partial arcs bounded by steep inner scarp and gentle outer flank, like low crater rims. Intermediate ring or arcs indistinct. Inner, 360-km-diameter ring continuous but low. Deposits not observed.	Chapter 8; WE77.
NECTARIS	4.3W	16° S., 34° E.	4 M-71 4 M-83 4 M-84 HK62(r) 4 M-52	860 600 450 350	--- --- --- ---	Main topographic rim is well-defined scarp on west (Rupes Altai), discontinuous mare-embayed mesas on east. Intermediate ring broad and low, bifurcates in west, forms discontinuous plateaus in east. Inner ring diverse, low. Possible additional ring defined by mare border, 240 km in diameter. Deposits extend 650 to 950 km, typically 750 km, from center; secondaries extend 700 to 1,500 km.	Chapter 9; B49, HK62, WM71.
Australe	4.3X	51.5° S., 94.5° E.	4 M-9 4 M-11 4 M-118	880 --- ---	--- 275 95	Outer ring includes large massifs. Intermediate, poorly defined ring contains massifs, locally connected by rugged structure to outer ring. Inner "ring" consists of closed series of irregular elevations. No deposits observed.	Chapter 8; SH70, WE77, W79.
ORIENTALE	4.3Y 4.4 4.5	20° S., 95° W.	4 M-194(r) 5 M-19 5 M-22 See fig. 4.4	--- 930 620 480 320	650 --- --- --- ---	Most nearly complete concentric ring structure among large basins except in the west. Outermost conspicuous ring is Cordillera, bounded inwardly by steep scarp or gentle lip and topped by some ridgelike massifs. Semicircular depression is outside this ring, and a raised 650-km-radius ring may be east of basin. Extension of Cordillera west of basin merges with extensions of Rook (620 and 480 km diam) rings as rugged, irregularly structured upland. Other sectors of outer Rook ring consist of large massifs with steep inner and gentler outer slopes in a sawtooth pattern. Large section of inner Rook ring and small section of 320-km-diameter ring also have large massifs; otherwise, inner Rook ring consists of smaller massifs or a steplike lip, and 320-km-diameter ring is defined by a lip or gradual falloff. Knobby hills suggest a plateaulike central uplift. Radial structures in inner basin. Extensive ejecta and secondaries.	Chapters 4, 10; HK62, B63, M67.

TABLE 4.1.—*Definite lunar basins at least 300 km in diameter—Continued*

Basin	Figure	Center (lat, long)	Best photographs	Major rings: Diameter (km)	Major rings: Radius (km)	Description	References
CRISIUM----------	4.3Z 4.9	17.5° N., 58.5° E.	4 H-191 HK62(r) 4 M-21 4 M-60	1,060 --- --- 635 500 380	--- 450 380 --- --- ---	Outer ring consists of three differently expressed segments: rimlike scarp in north, ridge bordering a trough in northwest, and irregular scarp in southeast. Elevations fall off inward from this ring, which also marks start of secondary chains. Ridges inside northwest ridge and massifs inside southeast scarp are about 380 and 450 km in radius, respectively, but are not closely concentric. Main mare-bounding rim is most conspicuous structure, divisible into 500- and 635-km-diameter rings, the inner consisting of large massifs with missing sector in east, and the outer of high but irregular massifs and other ridges and hills, separated from inner ring by deep irregular depressions. Innermost ring defined by a mare bench and small hills. Deposits and secondary craters extensive to east (1,600 km from center?), secondaries extensive to north (900 km) and south (1,100 km).	Chapter 9; HK62, SH70, WM71, WE77.
IMBRIUM----------	4.3AA	33° N., 18° W.	4 M-115 4 M-139 HK62(r)	--- 1,160 670	900 --- ---	Center as shown and 1,160-km ring are formed by Montes Carpatus, Apenninus, and Alpes. North shore of Mare Frigoris has 900-km radius from same center and is another major rim; both parts connect with Montes Caucasus. Lineations in Caucasus radial to same center. Montes Recta and Spitzbergensis and mare ridges define 670-km-diameter ring about a more northerly center; other connections are less certain and not given here. Lineate ejecta is north of Frigoris and south and southeast of Carpatus-Apenninus (Fra Mauro Formation); knobby ejecta (Alpes Formation) is closer to rings in all sectors, imbricate on south Apenninus flank (material of Montes Apenninus). Secondary craters abundant in all exposed sectors to 1,400-2,700 km from center, typically to 2,300 km.	Chapter 10; G93, B49, B63, HK62, SH62, WM71.
South Pole-Aitken------	8.8	56° S., 180°	---	2,500 ---	--- 900	Huge massifs and scarps define single rim averaging 2,200 km in diameter, or two rings about 2,500 and 1,800-2,000 km in diameter.	Chapter 8; S78, W79.

TABLE 4.2.—*Probable and possible lunar basins at least 300 km in diameter*

[Basins named by convention described in table 4.1. All basins are pre-Nectarian (see chap. 8) except possibly Sikorsky-Rittenhouse (Nectarian?). Diameter refers to outer or only observed ring. References: B63, Baldwin (1963); B69, Baldwin (1969); C74-81, Cadogan (1974, 1981); HH77, Hawke and Head (1977b); MA81, Maxwell and Andre (1981); SH70, Stuart-Alexander and Howard (1970); WE77, Wilhelms and El-Baz (1977); WM71, Wilhelms and McCauley (1971); W79, Wilhelms and others (1979); W81, Whitaker (1981)]

Basin	Map symbol (pl. 3)	Center (lat, long)	Figure	Apparent diameter (km)	Evidence and status as basin	References
Pingré-Hausen----------	PH	56° S., 82° W.	1.9	300	Arcuate ridges adjacent to Mendel-Rydberg; possibly part of that basin----------	Pingré of HK62 and HW71; W79.
Sikorsky-Rittenhouse----	SR	68.5° S., 111° E.	1.5	310	Craterlike rim and inner hills. Buried by Schrodinger deposits; possibly part of South Pole-Aitken basin.	B69; "unnamed A" of HW71; W79.
Amundsen-Ganswindt------	AG	81° S., 120° E.	1.5	355	Craterlike rim and trace of inner ring. Buried by Schrödinger deposits; possibly part of South Pole-Aitken basin.	B69, W79.
Werner-Airy-------------	WA	24° S., 12° E.	8.12	500	Indistinct low ridges bordered by depressions. Doubtful basin----------	B63, p. 195; named here.
Balmer-Kapteyn----------	BK	15.5° S., 69° E.	1.5	550	Concentration of plains inside and around rugged arcuate hills. Two rings may be exposed. Probable basin.	Balmer basin of MA81; renamed here.
Flamsteed-Billy---------	FB	7°-8° S., 45° W.	8.10	570	Semicircular arrangement of terra islands and part of Procellarum shore. Possibly part of Procellarum basin or craters.	WM71; named here.
Marginis----------------	Ma	20° N., 84° E.	9.4	580	Terra arcs and outline of Mare Marginis. Possibly part of Crisium basin--------	WE77.
Al-Khwarizmi/Xing-------	AK	1° N., 112° E.	8.11	590	Mostly elevations of crater units; one distinct ridge in northwest sector. Doubtful basin.	WE77.
Insularum---------------	In	9° N., 18° W.	8.10	600	Islands south of Montes Carpatus, deflections of Montes Carpatus, and coarse terra structure east of Sinus Aestuum. Possibly part of Procellarum.	WM71; "South of Imbrium" of HH77; named here for Mare Insularum.
Grissom-White-----------	GW	44° S., 161° W.	8.15	600	Elevated terra ridges and mare concentrations. Possible external structure of Apollo.	Named here.
Lomonosov-Fleming-------	LF	19° N., 105° E.	8.13	620	Partly complete circle of ridges; concentration of plains. Probable basin------	WE77.
Mutus-Vlacq-------------	MV	51.5° S., 21° E.	8.12	690	Distinct massifs and ridges in south; concentration of plains. Probable basin.	W79.
Nubium------------------	Nu	21° S., 15° W.	1.8	690	Conspicuous rim east of Humorum; arcuate margin of south-central terra. Probable basin.	SH70, WM71.
Tsiolkovskiy-Stark------	TS	15° S., 128° E.	1.3	700	Isolated terra ridges and elevated crater rims. Indistinct----------	B69, WE77.
Tranquillitatis---------	Tr	7° N., 40° E.	1.1, 1.7	800	Arcuate mare-terra boundary, especially in west. Probable basin----------	SH70, WM71.
Fecunditatis------------	Fe	4° S., 52° E.	11.17	990	Three possible rings: arc, 990 km in diameter, in northwest sector; main mare/terra boundary, forming circle 690 km in diameter; and circular mare ridges. Southward extension of mare mostly inside 990-km-diameter ring. Probable basin.	SH70, WM71, WE77.
Procellarum------------	P1, P2, P3	26° N., 15° W.	8.10	3,200	Terra ridges, mare/terra boundary, mare ridges, influence on later geology (see chaps. 5, 6, 11-13).	W81; similar to Gargantuan basin of C74-81.

Because of the pivotal role played by investigations of Orientale both before and after the Apollo 16 mission, Orientale deposits are taken as models for others and are thoroughly described in this chapter. Similarities to the Orientale deposits appear repeatedly in the rest of the terrae and reveal the presence of basin deposits in all degrees of preservation from the fresh to the barely discernible.

Although all primary-impact excavations are surrounded by basically similar ejecta and secondary craters, their interior morphologies differ sharply from the small to the large end members of the impact series (figs. 3.2, 4.2, 4.3). Morphologic complexity increases most obviously in the simple-to-complex transition at diameters of about 20 km and again at diameters of about 300 km. Like the first, this second transition has exceptions. All unburied lunar impact cavities larger than 300 km in diameter display interior rings; however, some cavities smaller than 300 km also contain rings. Antoniadi (135 km diam) and Compton (162 km diam) each have a peak centered inside an inner ring. Schwarzschild (235 km diam) has a partial ring, and Milne (262 km diam) has several. Several craters display ringlike patterns of internal peaks (figs. 3.2*E*, 4.2*C–E*). Some tectonically modified craters appear to possess a concentric structure (see chap. 6). On the other hand, several partly buried circular depressions larger than 300 km in diameter do not display the expected second ring.

These deviations muddy the definition of the term "basin." All authors agree that cavities larger than 300 km in diameter that have concentric rings instead of central peaks are basins, but opinions differ about whether this definition should be based entirely on size or on the presence of a second ring regardless of size (Wood and Head, 1976). This chapter concentrates on excavations at least 300 km in diameter, and classifies those without observed interior rings as indefinite basins (table 4.2). The problem of nomenclature for transitional features smaller than 300 km is not resolved here.

The origin of rings is among the most important unsolved problems of lunar geology. Orientale is also critical to this problem. Its four major rings are the most regularly spaced on the Moon (fig. 4.3). The 930-km-diameter Montes Cordillera ring, partly scarplike and partly topped by massifs, bounds the basin (figs. 4.1, 4.4). Two jagged massive rings, collectively called Montes Rook, have diameters of 480 and 620 km and lie inside the Cordillera. The fourth, innermost ring, 320 km in diameter, consists partly of scarps and partly of massifs. A low fifth ring, 1,300 km in diameter, outside the Cordillera has also been suggested (Hartmann and Kuiper, 1962). Each ring is 1.3 to 1.5 times larger than the one inside it, an interval that has been generalized as the square root of 2 (Hartmann and Wood, 1971). Although they are more regular than they are typical, as I will show below (compare figs. 4.4, 4.5), the Orientale rings are generally taken as the model for the spacing and formation of other rings in most of the literature, including the section below entitled "Origin of Rings."

Central to the controversy is the identity of the boundary of excavation. Some investigators, including myself, believe that the excavation cavity of basins which corresponds to the excavation cavity of simple craters is approximately the present basin itself, that is, the depression. The *topographic basin rim* that bounds most of the basin depression thus corresponds to the rim crest of simple craters. The topographic rim of Orientale is the Cordillera. In this hypothesis, the topographic rim bounds the excavation cavity and marks the inner boundary of the most voluminous ejecta. Many other investigators, however, believe that the primary, original cavity was smaller than the present basin. They identify the boundary of the excavation cavity with one of the interior rings or place it at a radial position formerly occupied by a raised ring and now by a trough. Stratigraphic questions that could be better answered by knowing the identity of the boundary include: (1) the position of the lithologic boundary between the ejecta and the interior deposits, (2) the volume of excavated material, (3) the ejecta's source depth in the terra crust or mantle, (4) the amount of melt generated by the impact, and (5) the position of the facies change between primary ejecta and ejecta of the secondary craters.

ORIENTALE EXTERIOR

By John F. McCauley

General features

The exterior ejecta deposits of Orientale form nearly concentric zones similar to the concentric facies of crater materials. In proportion to cavity size, the extent of morphologically similar facies is the same for both basins and large craters (Moore and others, 1974; Morrison and Oberbeck, 1975). A continuous deposit extends outward an average distance of 450 km, or one basin radius, from Montes Cordillera. Beyond this deposit, clustered secondary craters accompanied by their ridgelike and planar ejecta form a more varied terrane of discontinuous deposits. In some sectors, dense concentrations of secondaries extend 900 km (two basin radii) from the Cordillera; secondaries also extend beyond 1,850 km in at least one raylike string (fig. 4.6; Wilhelms and others, 1978, p. 3752), much like secondary clusters along the bright rays of young craters. The most conspicuous deposits of all types are shown on plate 3, and the continuous and discontinuous deposits are distinguished.

The continuous deposits closest to the rim and the discontinuous deposits at greater distances are collectively designated the Hevelius Formation, the first stratigraphic unit whose relation to Orientale was recognized (McCauley, 1967a, b). This definition was based on telescopic observations and was originally applied to a tract centered around lat 2° N., long 68° W., that is now considered part of the outer facies. Scott and others (1977) later expanded the definition to include the continuous, more coarsely textured blanket farther west, which had also been detected telescopically (McCauley, 1964b). The Hevelius and other Orientale materials, except the plains materials also discussed here, collectively constitute the Orientale Group (McCauley, 1977; Scott and others, 1977).

Inner facies of the Hevelius Formation

The continuous deposits of the Hevelius Formation form an enormous doughnut-shaped zone, elongate north-south and from 300 to at least 600 km wide, outside Montes Cordillera (pl. 3; figs. 1.9, 4.1, 4.4*A–G*; Scott and others, 1977). This zone is difficult to delineate west of Orientale because of the obliquity and poor quality of the Lunar Orbiter 5 photographs of that area (pl. 3*B*; fig. 4.5). However, this part of the Hevelius, called by Scott and others (1977) the inner facies of the Hevelius Formation, is generally the most distinctive unit of the Orientale Group. It displays abundant attributes of a massive ejecta deposit that acquired a distinctive textural imprint during flow along the rugged prebasin surface.

The inner, continuous Hevelius is texturally characterized by elongate ridges and irregular troughs generally radial to Orientale; figure 4.4*C* shows a typical locality. The ridges are curvilinear and mutually crosscutting; some ridges have nearly streamlined forms, and others appear ropy or filamentary. These landforms clearly resulted from surface flow of deposits differentially affected by obstacles. Some of the larger ridges have lobate edges that resemble the fronts of viscous flows of lava or debris (fig. 4.4*D*). Numerous narrow linear grooves are also visible, particularly in the lower and smoother parts of the deposits. Another characteristic are the myriads of vague elongate depressions and chains of depressions, visible only in good photographs, that are overlain by ridged and grooved materials (fig. 4.4*C*). The shapes, subdued appearance, and distribution pattern of these depressions indicate that they are secondary craters, partly or completely buried by slightly later flows of ejected deposits. Although these buried secondary craters contribute a negative-relief pattern, the generally larger positive forms dominate the scene. Their distribution pattern and topography argue for strong centrifugal depositional movements within the materials that make up the inner, continuous Hevelius.

The inner facies of the Hevelius Formation generally forms a continuous ground cover that deeply buries or subdues large primary craters on the pre-Orientale surface (figs. 4.1, 4.4*F*, *G*). The depth of burial of these craters generally decreases outward from the basin. Estimates based on the depth of crater burial indicate that the inner facies of the Hevelius decreases in thickness from 3 to 4 km near Montes Cordillera to no more than several hundred meters at its outer edges (Moore and others, 1974). However, these estimates assume that the buried craters had the *d*/*D* ratios of fresh craters, which compose only part of any random population of lunar craters. Theoretical models of ejecta thickness (McGetchin and others, 1973) are also very uncertain in view of the number of simplifying assumptions that underlie them (Solomon and Head, 1979, p. 1669). Calculations are hampered by uncertain cavity volumes, uncertain degree of bulking of the ejected material (Croft, 1978), and the difficulties of scaling from one gravity field to another (Gault and others, 1975). Basin deposits are visibly irregular and lobate (pl. 3), and are not equally thick all around a basin at a given radial distance. Thus, their thicknesses are poorly known but are probably less than 4 km.

The well-developed radial or semiradial trends prevail within most of the inner facies of the Hevelius except in a sector of about 50° of arc east of the basin (figs. 4.4*E–G*). This anomalous region has little radial texture and is part of the concentric facies of Moore and others (1974), who noted an outward gradation here and elsewhere from this concentric facies to more nearly radial material (top, fig. 4.4*F*). The inner Hevelius in the anomalous area (fig. 4.4*F*) has stubbier ridges and lobes than in more typical localities (figs. 4.4*C*, *D*, *G*). Large patches of smooth to rolling weakly lineate terrain are also present, some of which show numerous small ridges and troughs concentric with the basin. In addition, the depressions formed by buried secondary craters are not so large and do not contribute so significantly to the surface texture as in more typical parts of the inner Hevelius (figs. 4.4*C*, *D*, *G*). The long axes of many of these depressions are also concentric rather than radial to the basin. Prebasin craters are not so deeply buried as in the more strongly radial parts of the Hevelius Formation at comparable distances from the basin. All indications in this sector point to ejection of less material at lower velocities than elsewhere.

Small patches of what has been described as the fissured facies and interpreted as impact melt (Moore and others, 1974) occur within the inner facies of the Hevelius. These smooth but locally fractured deposits lie in depressions and contrast sharply with the topography of their surroundings (fig. 4.4*B*); they also are somewhat darker than the adjacent material. Their patterns of fissures resemble those caused by shrinkage of a coherent material. These small deposits (areas less than a few tens of kilometers on a side) are widely scat-

tered, and are included in the inner facies of the Hevelius on the map by Scott and others (1977) and in the inner Orientale unit on plate 3. They resemble the smaller impact-melt pools on the flanks of craters (figs. 3.23, 3.27, 3.36).

In mapping the Orientale region at 1:5,000,000 scale, Scott and others (1977) distinguished a transverse facies of the Hevelius Formation, also included here in the inner Orientale zone (pl. 3). This transverse facies consists of patches of closely spaced, ropy-looking, intertwined ridges and intervening troughs arranged concentrically around Orientale. Typical dimensions of these patches are about 30 by 60 km. They are common on the far sides of crater floors (figs. 4.4*F–H*) 300 to 600 km from Montes Cordillera. They seem to be more abundant on the east side of the basin, but this apparent asymmetry may be due to the poor photographic coverage of the west side (fig. 4.5). These subparallel features, which have been termed "deceleration dunes" (McCauley, 1968), are good evidence for the surface flowage of Orientale ejecta. In the crater Riccioli, transverse ridges are banked up on the far side of the crater floor, beyond which a transversely textured flow lobe, 100 km long, emanates from a breech in the distal crater wall (fig. 4.4*H*). The influence of topography on several patches of less well defined transversely textured materials is less obvious (figs. 4.4*F–H*).

The inner boundary of the Hevelius Formation has been perceived both as sharply demarcated by Montes Cordillera (Baldwin, 1974a; Wilhelms and others, 1977; Hodges and Wilhelms, 1978; Murray, 1980) and, alternatively, as irregular, gradational, and not everywhere coincident with Montes Cordillera (McCauley, 1977; Scott and others, 1977). Much of the Cordillera scarp is draped by the Hevelius Formation (figs. 4.4*A–F*). Locally, however, sharp breaks in texture mark the inner contact of the Hevelius along the steeper parts of the Cordillera scarp, particularly where this scarp is shadowed on photographs (fig. 4.4*E*).

Outer facies of the Hevelius Formation and secondary craters

The outer facies of the Hevelius Formation (Scott and others, 1977), like the outer parts of all ejecta blankets, exhibits a greater variety of surface textures than the inner facies. The facies boundary is gradational but readily detectable on good photographs as the limit of the large radial lobate ridges typical of the inner facies of the Hevelius (figs. 4.4*G, H*). This contact is reproducibly mappable within a few tens of kilometers on the nearside but is hard to detect on the farside. Subdued, elongate, sinuous to irregular secondary-crater depressions typical of the inner facies are replaced in the outer facies by crisp secondary craters that are not overrun by ejecta. Buried prebasin primary craters are also more conspicuous in the outer than in the inner facies. Large patches of smooth plains also become abundant near the facies boundary and interrupt the radial depositional patterns. The boundary is analogous to that between the continuous inner deposits and the herringbone-patterned fields at one crater radius from the rim crest of craters.

The tract near the type area of the Hevelius Formation (McCauley, 1967a) contains faintly lineate, thin, and discontinuous material that mantles the wall of the crater Hevelius nearest to Orientale and grades to smooth plains on the crater floor. The adjacent high ground shows numerous relatively straight grooves and ridges, in contrast to the larger and more sinuous topographic forms of the continuous Hevelius. Some of these smaller and straighter grooves locally resemble mantled grabens but were probably created during emplacement of the Hevelius Formation (loc. 2, fig. 4.4*H*). Obvious depositional patterns are subordinate or absent, and this "lineated terra material" (Wilshire, 1973) or "grooved facies" (Moore and others, 1974) has been considered to be partly of erosional origin. However, depositional origins and erosional or secondary-impact origins are difficult to distinguish where the grooves are separated from terrain with more diagnostic features (Wilhelms, 1980).

In many places, the outer facies of the Hevelius Formation is rolling to hummocky and furrowed, particularly near the crater Crüger and eastward to Oceanus Procellarum (fig. 4.4*H*). This terrane generally shows only vague radial lineations and elongate depressions, as well as numerous subdued pits. Although a secondary-impact origin for this hilly and pitted terrain was mentioned (McCauley, 1973), a volcanic origin was preferred before the Apollo 16 results were obtained (Wilhelms and McCauley, 1971; McCauley, 1973; Wilshire, 1973). Continued studies have shown that the strange-textured terrane is laterally continuous with Hevelius deposits similar to those shown in figure 4.4*F* (Scott and others, 1977). The terrane probably consists of a pre-Orientale surface mantled by Orientale ejecta that had less radial momentum or velocity than other parts of the blanket.

Although some deposits and grooves are of primary-ejecta origin and others of doubtful origin, the outer zone of Orientale materials mapped here (pl. 3*A*) is clearly characterized by the products of secondary impacts. Obvious secondary craters large enough to map at 1:5,000,000 scale were considered by Scott and others (1977) as a separate facies of the Hevelius Formation, but secondary craters are not mapped separately from deposits here (pls. 3, 6–8). Secondary craters of Orientale were described by Offield (1971), Wilhelms and McCauley (1971), Moore and others (1974), and Wilhelms (1976) (see chap. 3). The Orientale secondaries overlap in chains and clusters that are scaled-up equivalents of the secondaries described around Copernicus by Shoemaker (1962b). Diameters of individual craters are as large as 28 km, but most are from 7 to 20 km (Wilhelms and others, 1978), typically about 10 km (figs. 3.9, 4.4*C, G, H*). Although some distant clusters have downrange herringbone patterns (fig. 3.9), these patterns are subordinate to straight ridges nearly radial to the basin (figs. 4.4*G, H*). Bowl-shaped to elongate gougelike features are typical of the Orientale-secondary field. Their downrange sides show wavy or partly braided deposits that partly or completely obscure the underlying topography. Many individual craters have well-developed rims and appear to be moderately fresh; others are very subdued and have been mistaken for prebasin craters (figs. 4.4*G, H*; Wilhelms, 1976). Orientale secondaries, including some that extend great distances from the basin (fig. 4.6), are abundant beyond a large lobe of the Hevelius Formation southeast of the basin (pl. 3; fig. 4.4*G*). Secondaries are especially large and abundant north of the basin (fig. 3.9) and on the poorly photographed west side (fig. 4.5), but are rare in the concentrically textured sector east of the basin (figs. 4.4*E–G*).

The outer facies of the Hevelius Formation, like the outer parts of all impact-crater deposits, represents a progressively thinner to more discontinuous cover that may locally extend to great distances from Orientale without leaving a perceptible imprint on the topography. The problem of identifying the outermost limit of ejecta is intrinsic to mapping all impact and explosion craters. Here, the outer contact is placed where no further linear or Orientale-radial structure can be observed on Lunar Orbiter 4 H-frames (pl. 3). Beyond this contact, only isolated secondary craters and crater clusters are recognizable as related to Orientale (figs. 4.6, 7.7, 10.5). Farflung Orientale ejecta could have reached points thousands of kilometers from the basin (Chao and others, 1975; Moore and others, 1974). It may even be concentrated in the furrowed and pitted terrain antipodal to Orientale near Mare Marginis (fig. 4.7; Schultz and Gault, 1975a; Wilhelms and El-Baz, 1977).

Relation between ground-flow deposits and secondary craters

As discussed above, numerous vague and irregular depressions, gouges, and clusters of radially lineate, buried secondaries occur within both the outer and inner facies of the Hevelius Formation (figs. 4.4*C, D, F, G*). Some chainlike secondary craters buried by the continuous Hevelius extend to the Cordillera ring (fig. 4.4*D*), as do similar chains at the double-ring Schrödinger basin (fig. 1.5). Surficial flow textures characteristic of the Hevelius Formation overlie these chains; thus, the chains were probably formed by early-arriving clots of ejecta traveling in relatively low ballistic trajectories from the basin, and were later overrun by a slower-moving ground surge (Morrison and Oberbeck, 1975; Oberbeck and Morrison, 1976). Morrison and Oberbeck (1975) suggested that most of the other radial and concentric depositional ridges of the inner facies of the Hevelius were created by interference and interaction of ejecta, as are the herringbone patterns around craters. Such an origin would imply that the ridges contain little primary basin ejecta. This process probably did form many of the ridges in the outer parts of the secondary field (figs. 3.9, 4.4*G, H*), but not the long sinuous ridges and grooves of the inner facies of the Hevelius, which were deflected by obstacles in a way that indicates surface flowage of thick ejecta (fig. 4.4*G*). Furthermore, the burial of the secondaries indicates that primary ejecta constitutes most of the inner facies; any secondary ejecta present there must have

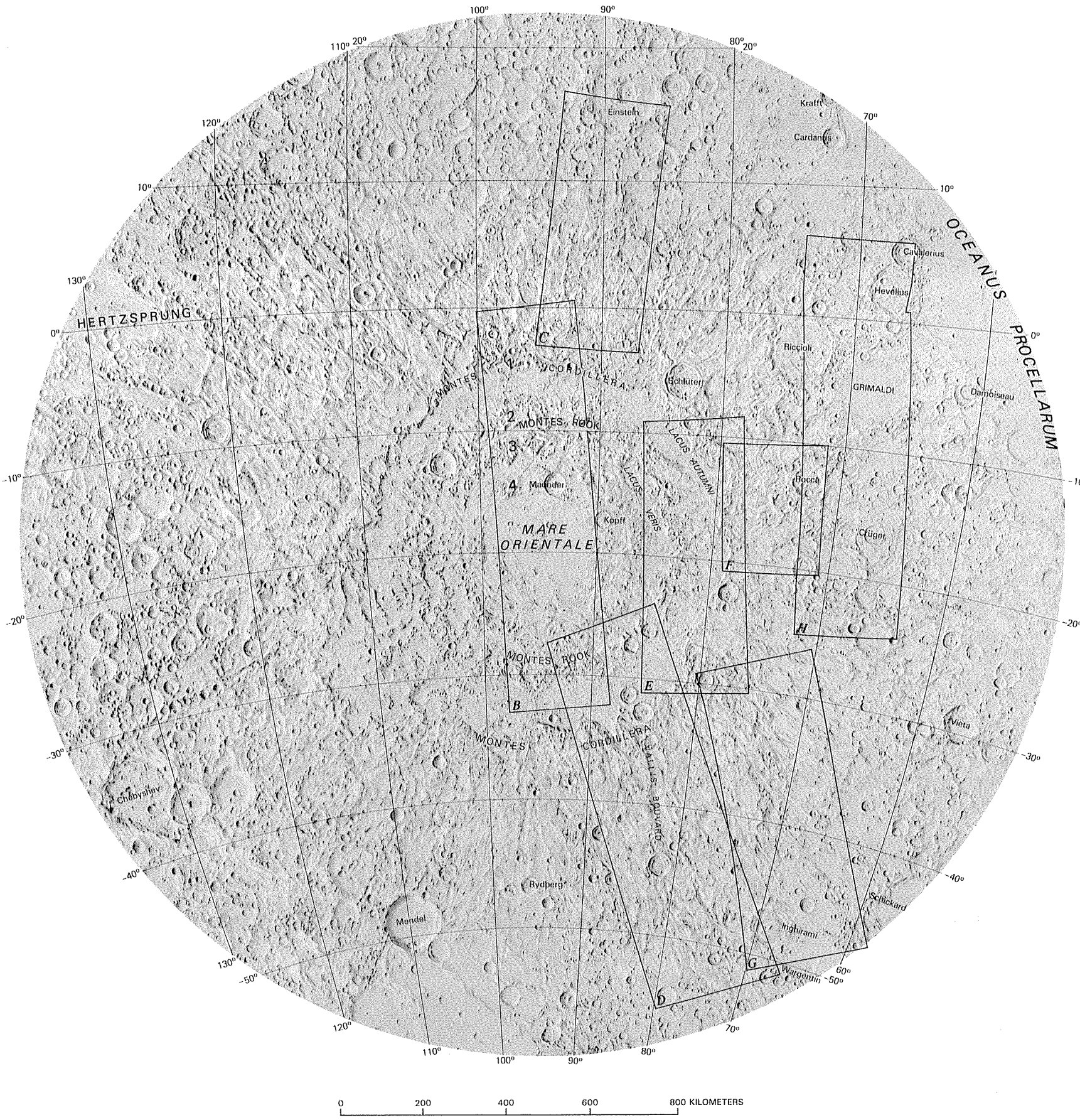

FIGURE 4.4.—Orientale basin and periphery.

A. Basin structure. 1, Cordillera ring (930 km); 2, outer Rook ring (620 km); 3, inner Rook ring (480 km); 4, innermost ring (320 km). After U.S. Geological Survey (1978).

B. Central Orientale basin, showing the Hevelius Formation (1), fractured impact melt (2), overlap of the Montes Rook Formation onto the Hevelius (3), Cordillera ring overlain by Hevelius (4) and Montes Rook (5) Formations, typical knobby Montes Rook Formation (6), outer Montes Rook ring massifs (7), inner Rook ring (8, 9a, 9b), massifs of 320-km-diameter ring (10), fissured domical Maunder Formation burying part of 320-km-diameter ring (11), and level Maunder Formation cut by grabens (12). Inner Rook ring massifs in south (9b) are widely separated by the Maunder Formation. Perched former higher stands of level part of the Maunder indicate subsidence (13). Orientale-basin materials are exposed from beneath shallow mare near center of basin (14). Circular structure of outer Rook ring (15) is possibly derived from prebasin crater. Crater Maunder overlies basin and mare (16). Orbiter 4 frame H–195.

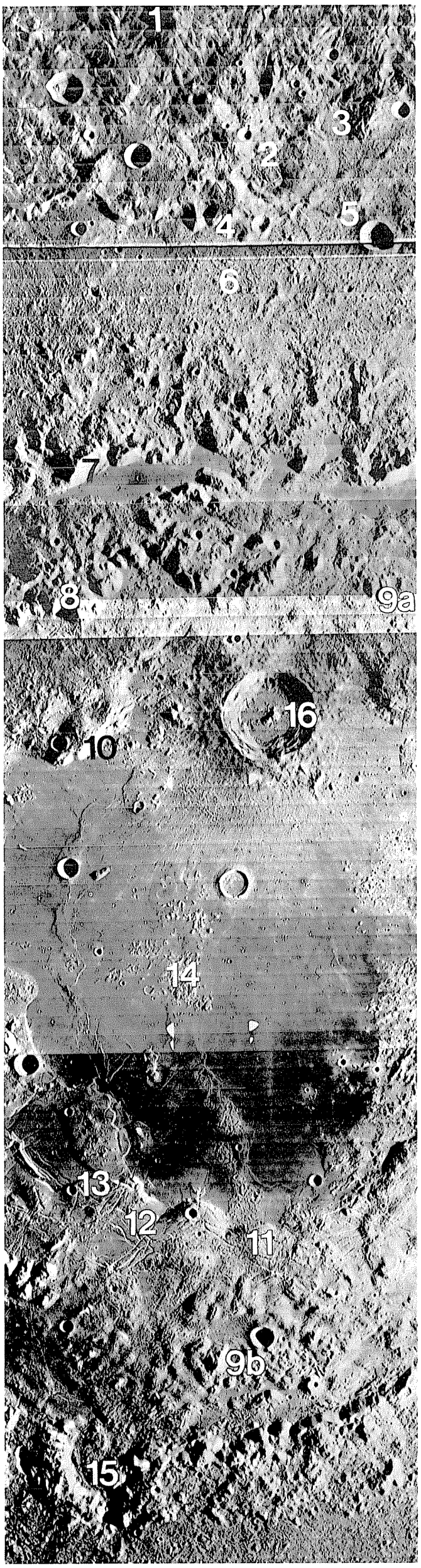

B

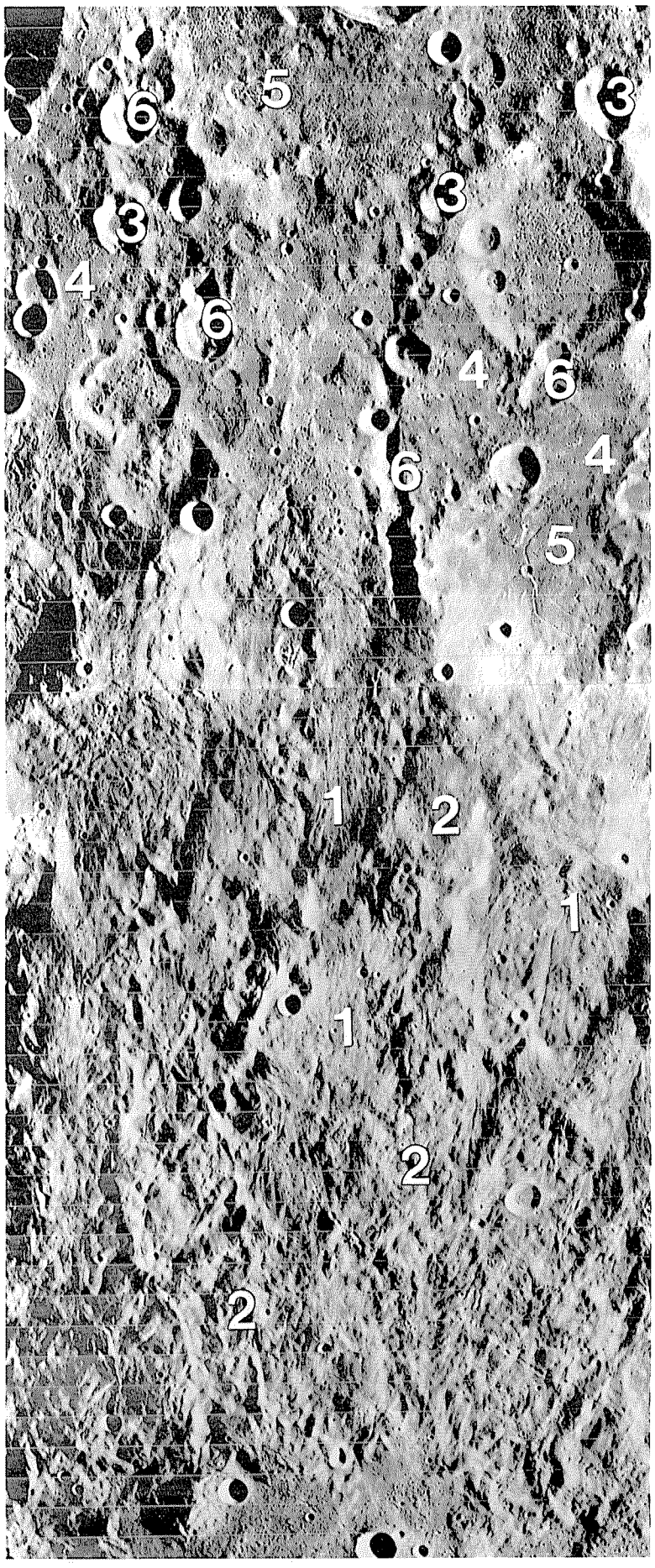

C. Typical continuous inner facies of the Hevelius Formation (bottom half of photograph). Many ridges are flow features (1); depressions are buried secondary craters (2). Large secondaries (3) emerge among smooth deposits (4) farther from basin. Fissures indicate possible melt deposits (5). Complex landforms were generated by multiple near-simultaneous secondary impacts (6). Overlaps with figure 3.9*A*. Orbiter 4 frame H–188.

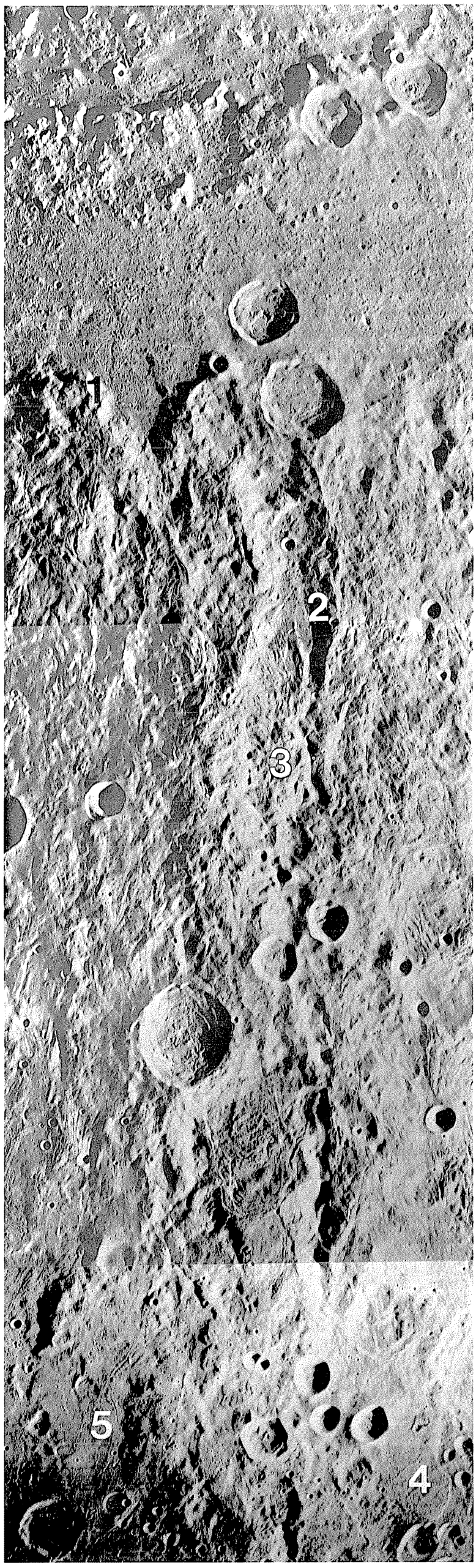

D

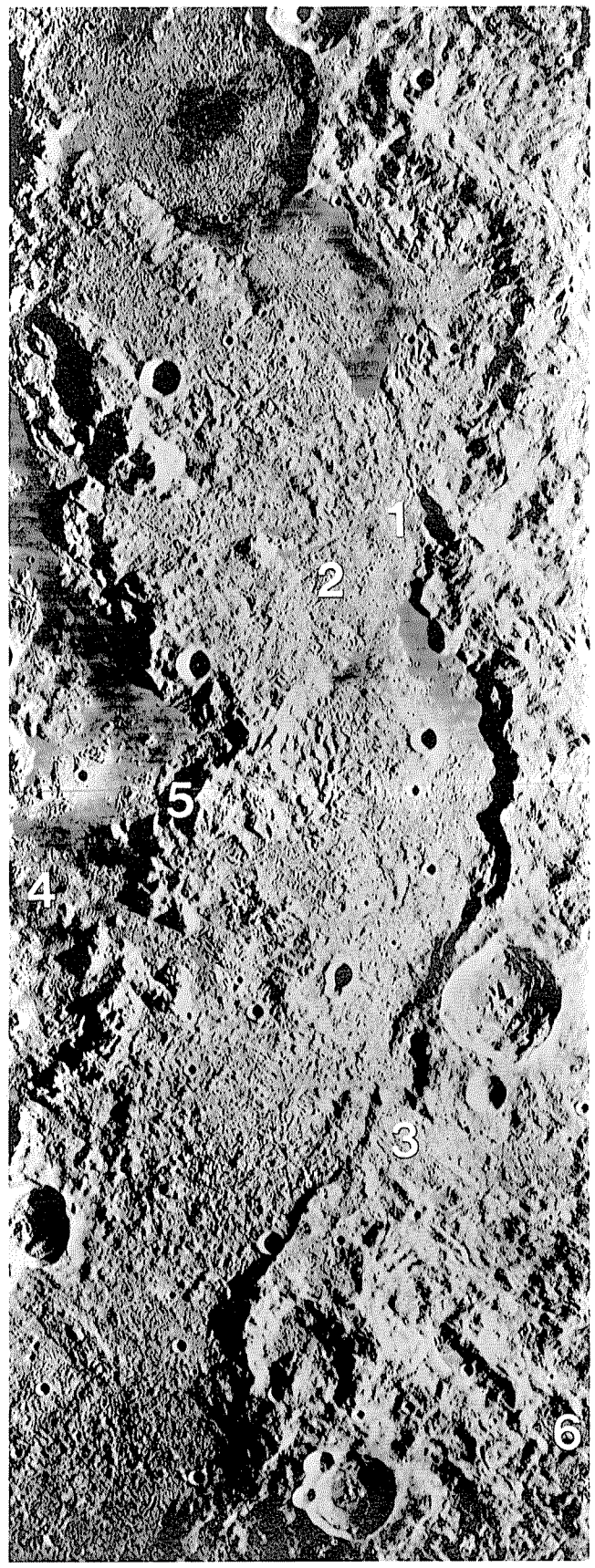

E

D. Cordillera ring (1) south of basin, overlain by chain of Orientale-secondary craters, Vallis Bouvard (2). Hevelius Formation mantles the secondary chain and extends outward as a thick blanket (3). Lobes of nonlineate (4) or leveed (5) material continue the Hevelius deposit outward. Orbiter 4 frame H–186.

E. Montes Rook Formation, decelerated by Cordillera ring into dunelike (1) or radially textured (2) deposits. Montes Rook or Hevelius Formation, with radial textures, overlies Cordillera scarp (3). Maunder Formation is at left (4), inside outer Rook ring (5). Fissured ejecta (6) is probable impact melt. Orbiter 4 frame H–181.

F. Radial (1) and concentric (2) textures of the Hevelius Formation directly east of Cordillera ring (3). Flow of the Hevelius was blocked by crater Rocca and piled up as dunelike mounds (4). Orbiter 4 frame H–173.

G. Transition between inner (1) and outer facies of the Hevelius Formation. Outer facies includes secondary craters (2), ridged deposits of secondaries (3), and planar deposits (4). Flow of the Hevelius was diverted by now-buried obstacles (5) and blocked by crater Inghirami (6). Some secondary craters filled by deposits look deceptively old (7). Orbiter 4 frame H–172.

H. Type area of the Hevelius Formation, centered at 1.7° N., 68.5° W. in crater Hevelius (1). Linear troughs radial to Orientale are partly filled by deposits (2). Deposits were decelerated by rim of crater Riccioli (3), but lobe of textured deposits extends northeastward of rim (4). Lobe of plains deposits inside Grimaldi (5), playout of decelerated deposits (6; same as at loc. 4, fig. 4.4*F*) into planar deposits (7), and pitted terrain (8) are also related to Orientale. Postbasin features: grabens (9), crater Crüger (10), and other mare-filled depressions (11). Mosaic of Orbiter 4 frames H–168 (bottom) and H–169 (top).

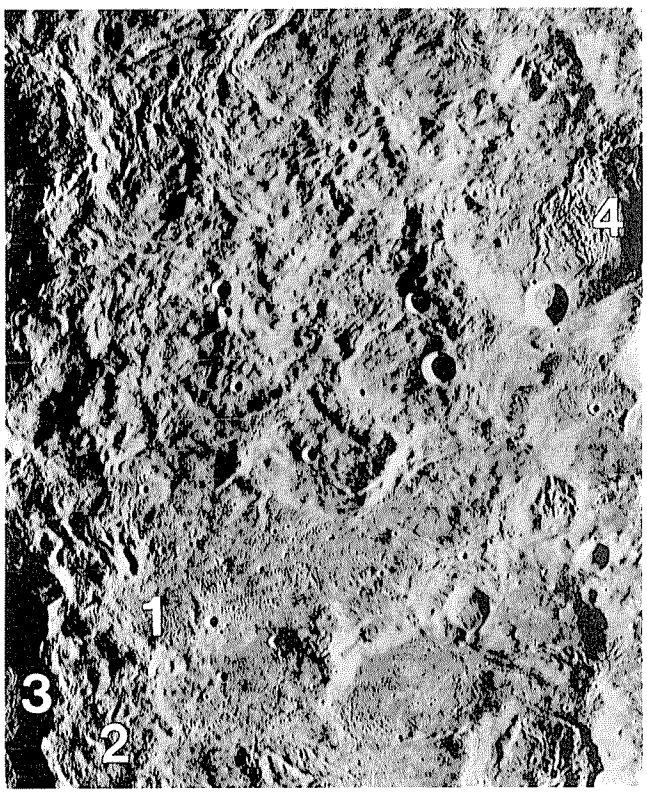

F

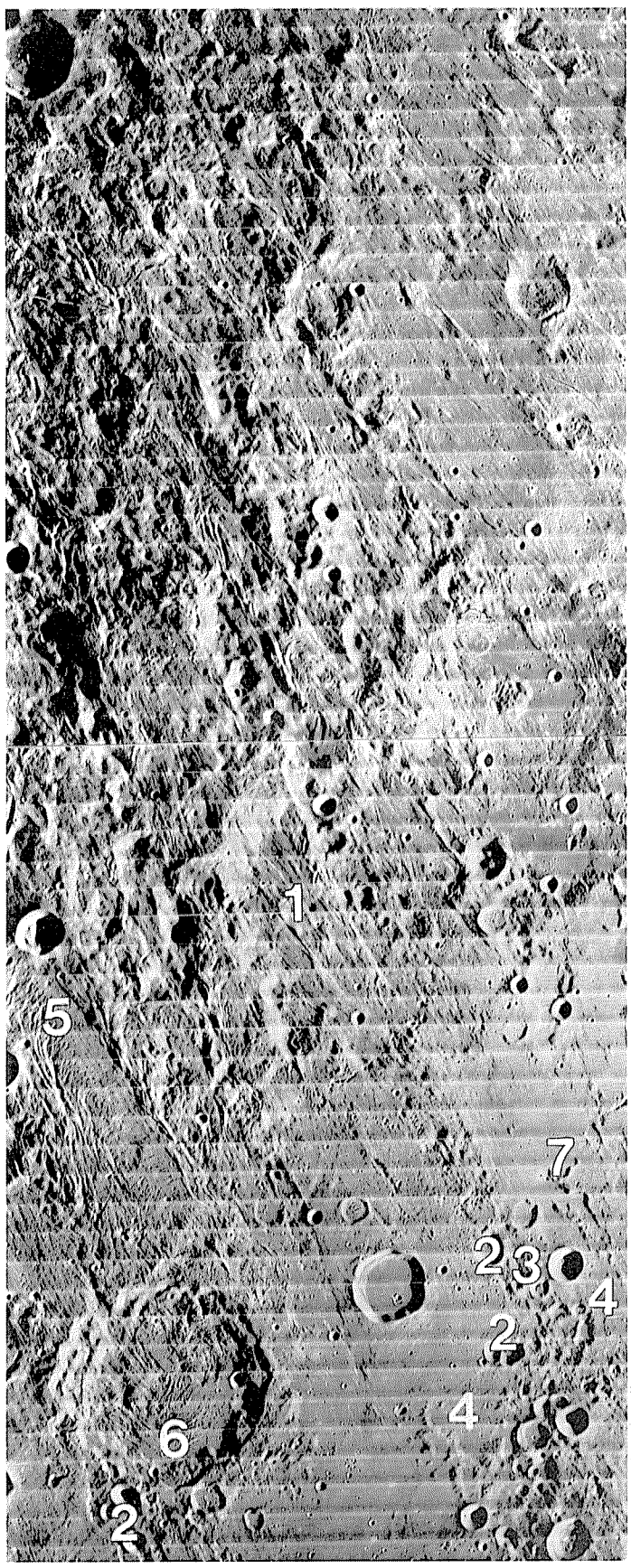

G

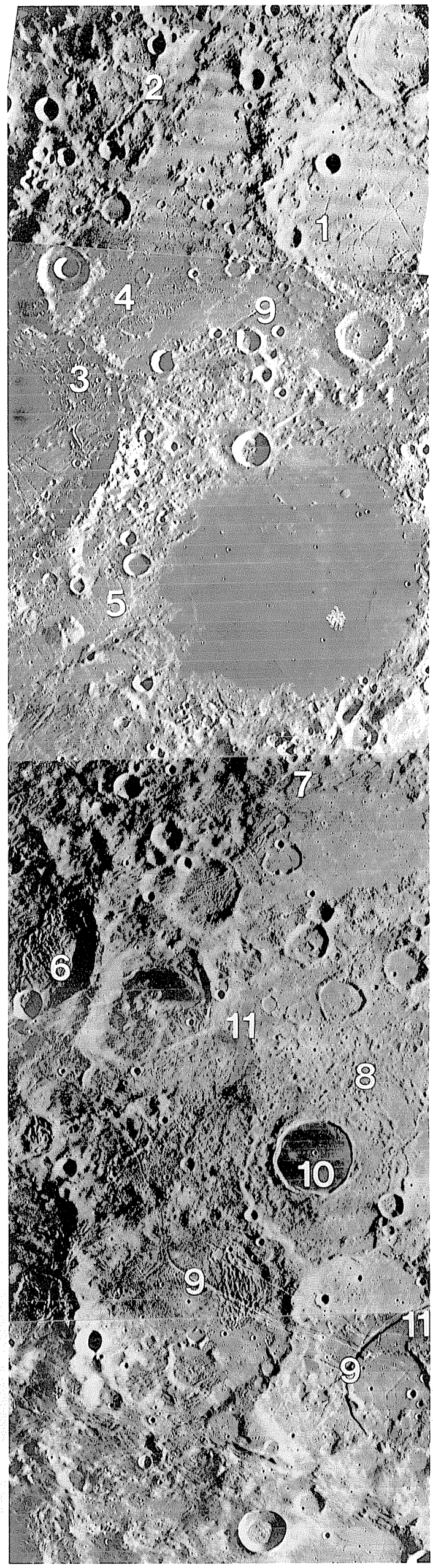

H

been overwhelmed by the primary ejecta. This question of the proportions of primary versus secondary ejecta in basin deposits is explored in discussions of the Apollo 14 and 16 samples in chapter 10.

The photographic evidence, therefore, suggests an early stage of secondary cratering followed by a ground-hugging debris surge that first inundated and then mixed with the earlier debris. The last-formed Orientale features, however, may also be secondary craters. Unusually numerous, crisp circular craters, 10 to 15 km in diameter, which at first glance appear to be primary craters younger than Orientale, are present in the west-limb region of the Moon (figs. 4.1, 4.4, 4.5). These may be very late secondary craters excavated by projectiles that were ejected from the Orientale basin at high angles and that almost reached escape velocity (as proposed by Shoemaker and others, 1968, p. 40-44, for craters on the rim of Tycho). Circular craters, presumably formed by high-velocity impacts, should be widely dispersed over the Moon not only from Orientale but also from all the older basins (figs. 4.6, 4.7).

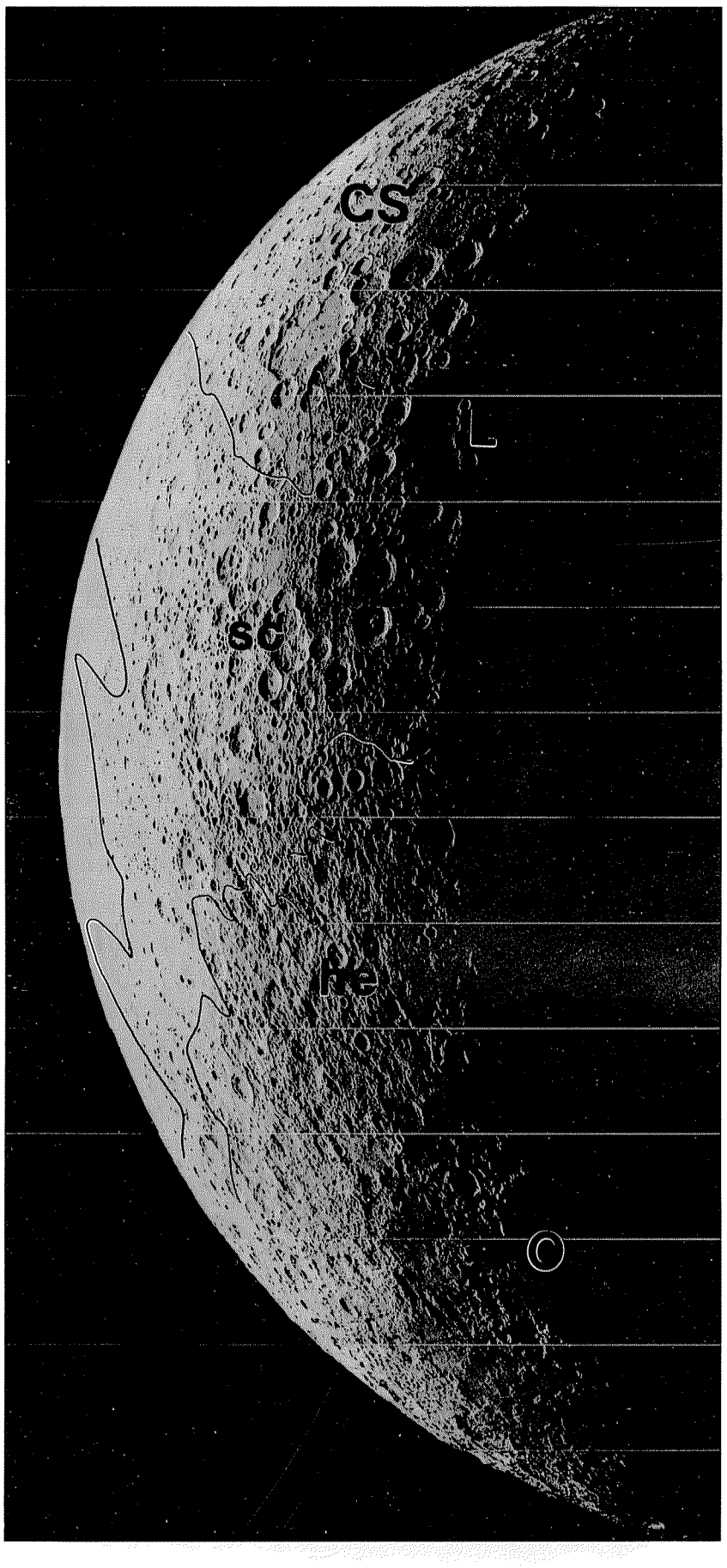

FIGURE 4.5.—West and northwest sectors of Orientale basin (O) on farside (compare fig. 4.1), showing radial pattern of continuous inner facies of the Hevelius Formation (he) and secondary craters (sc). CS, Coulomb-Sarton basin; L, Lorentz basin. Orbiter 5 frame M–16.

Plains

The Hevelius Formation is gradational with the terra plains. These plains are abundant in the transition zone between the inner and outer facies of the Hevelius and occupy additional large tracts in the outer facies. These relations have been much discussed since the discovery by Apollo 16 of impact breccia in similar light-colored plains in the central lunar highlands. Volcanic origins have been discounted in all but a few areas (see chaps. 2, 10; Neukum, 1977). The principal currently competing hypotheses are an origin as primary ejecta and as ejecta from secondary craters. Relations at Orientale provide the best photogeologic clues to the plains' origin.

Some nearly planar deposits have a distinguishable relief that is an important clue to their origin. Ridges of the inner facies of the Hevelius grade into faint rises in the plains of the transition zone (figs. 4.4*G*, *H*). Flat-topped lobes with planar or faintly textured surfaces (mapped as a separate nonlineated facies by Wilhelms and others, 1979) seem to have oozed from the more rugged Hevelius (fig. 4.4*D*; Eggleton and Schaber, 1972); some of these smooth deposits are leveed (loc. 5, fig. 4.4*D*; Hodges and others, 1973; Moore and others, 1974). Fluidlike flow of the semiplanar material is indicated. A substantial content of impact-melted rock may be responsible, although fluidlike flow of completely clastic debris is not excluded. Some textured deposits are superposed on secondary craters (figs. 4.4*D*, *F*). Little secondary ejecta can be contained in textured deposits with these stratigraphic relations.

By extension, fluidlike emplacement of material segregated from the textured ejecta blanket is suggested for the completely planar deposits that have ponded in depressions (Eggleton and Schaber, 1972). This origin is even likely for such deposits as those in the crater Wargentin (fig. 1.9), whose apparently thick fill was long considered to be evidence for lunar volcanism. The light-colored deposits in Wargentin lie just beyond the zone where the continuous Hevelius grades into the plains. Although Wargentin may have been partly filled by volcanic materials, the present surface deposit is probably of Orientale ejecta (Schultz, 1976b, p. 92).

Emplacement as secondary-crater ejecta, as hypothesized for all light-colored lunar terra plains by Oberbeck and others (1974, 1975), is likely for plains that lie far from the inner facies of the Hevelius but adjacent to clusters of secondary craters (fig. 7.6). The dispute between a primary and secondary origin for terra plains, therefore, is one not of exclusive genesis but of relative contributions by the two mechanisms.

The plains illustrate that the appearances and distributions of lunar geologic units may be consistent with more than one genetic interpretation. A further example is in the south-central highlands of the nearside, where careful mapping showed that plains and mantling deposits become less conspicuous from west to east (Cummings, 1972; Mutch and Saunders, 1972). The mappers interpreted the differences as due to variations in the thickness of the deposits, which they considered to be a function of the duration of volcanism. An impact interpretation, more consistent with current understanding of the lunar terrae, is that the plains are ejected materials which thin away from their source, Orientale.

ORIENTALE INTERIOR

By John F. McCauley

All or almost all the materials of the Hevelius Formation lie outside the topographic basin rim of Orientale (pl. 3). Additional Orientale deposits occur mostly in the basin interior or on the Cordillera rim close to the basin. Two major units are named the Montes Rook Formation and the Maunder Formation (fig. 4.8); these formations complete the Orientale Group (table 4.3; McCauley, 1977; Scott and others, 1977). Morphologic and, presumably, genetic analogs occur in craters (figs. 3.2*D*, 3.32–3.35) but are less conspicuous than in Orientale. Their analogs in other basins are less obvious than those

TABLE 4.3.—*Geologic units of lunar basins*

[Fm, Formation; n/n, recognized but not named; n/r, not recognized. Most units of other basins are named informally. References: H66, Hackman (1966); H74, Head (1974c); M74, Moore and others (1974); S71, Stuart-Alexander (1971); S77, Scott and others (1977); WM71, Wilhelms and McCauley, 1971; W79, Wilhelms and others (1979)]

Location	Morphology	Orientale (references)	Imbrium (references)	Nectaris (references)	Interpretation
Inner basin	Wavy, fissured	Maunder Fm (S77); corrugated facies (H74).	n/r	n/r	Impact melt, buckled.
Do	Level, fissured	Maunder Fm (S77)	Apennine Bench Fm(?) (H66).	n/r	Impact melt, fluid, little deformed.
Shelf and inner flank.	Knobby	Montes Rook Fm, knobby facies (S77); domical facies (H74).	Alpes Fm (WM71); Fra Mauro Fm, hummocky (H66).	Hilly material (WM71)	Late low-velocity high-angle ejecta.
Rim and other rings.	Massifs	Montes Rook Fm, massif facies (S77).	Rugged material (WM71)	Rugged material (WM71)	Upthrust and covered by ejecta.
Inner flank	Concentric, wreathlike.	Concentric facies (M74)	Fra Mauro Fm, hummocky (H66); material of Montes Apenninus (WM71).	n/r	Primary ejecta pushed over rim.
Flank	Radial, coarse	Hevelius Fm, inner facies (S77); radial facies (M74).	Fra Mauro Fm (H66, WM71)	Janssen Fm (S71, WM71)	Primary ejecta, flowed on surface.
Flank depressions.	Wavy, fissured	Fissured facies (M74)	n/n	n/r	Ejected impact melt.
Flank, transition zone.	Concentric, dunelike.	Hevelius Fm, transverse facies (S77).	Hilly material (WM71)	n/r	Primary ejecta, decelerated flow.
Do	Wide valleys	n/n (Vallis Bouvard type)	n/n	Material of crater chains and clusters (WM71).	Low-angle secondary impact.
Transition zone	Lobate, smooth or leveed.	Hevelius Fm, nonlineate member (W79).	n/r	n/r	Primary ejecta, fluidlike flow.
Do	Subcircular flat-floored craters.	n/n	Irregular-crater material (WM71).	Undivided crater material (WM71).	Secondary impact, filled by surface flow.
Transition, outer zones.	Narrow grooves	Grooved facies (M74)	n/n	n/n	Eroded by secondary impact or surface flow.
Do	Subcircular bowl-shaped craters.	Satellitic-crater material (WM71, W79); Hevelius Fm, secondary-crater facies (S77).	Material of crater clusters and chains (WM71).	Material of crater chains and clusters (WM71); satellitic crater material (W79).	Secondary impact.
Do	Radial, fine, linear, or braided.	Hevelius Fm, outer facies S77, W79).	Terra material (WM71)	Janssen Fm (S71, WM71)	Secondary-impact ejecta.
Do	Planar, smooth	Plains material or facies	Plains material	Pitted-plains material (WM71).	Primary or secondary ejecta, ponded.

of the exterior deposits because of mare flooding and other modifications. Thus, Orientale provides a unique opportunity for study of the interior materials of basins.

Montes Rook Formation

The Montes Rook Formation (or the knobby facies of that formation, Scott and others, 1977) is characterized by multitudinous smooth, equidimensional to elongate knobs, about 2 to 5 km across, set in a matrix of smooth to rolling materials (figs. 4.4*B*, *D*, *E*). In places, the formation contains weak lineations, mostly radial but locally concentric with the rings (fig. 4.4*E*); much of it has a ropy or imbricate texture. Most of the formation occurs between the Montes Cordillera and Montes Rook rings, although several large patches are exterior to the Cordillera (fig. 4.4*B*; Scott and others, 1977). Islands of lineate material, either belonging to the Hevelius Formation or intrinsic to the Montes Rook Formation, lie within the confines of the Montes Rook Formation (fig. 4.4*E*). Vague circular structures, less conspicuous than the large primary craters buried by the Hevelius Formation (fig. 4.4*B*), may be buried by the Montes Rook Formation (figs. 4.4*A*, *B–E*; Scott and others, 1977).

In places, the Montes Rook Formation appears to embay the coarsely lineate Hevelius (fig. 4.4*B*), and so the Montes Rook is the later unit in the basin sequence. Like the Hevelius, the Montes Rook material must have left the crater at least locally because it is so clearly draped over the Cordillera scarp (fig. 4.4*B*). Thus, it cannot be the product of inward slumping of the crater walls along the Cordillera scarp immediately or shortly after final excavation of the crater, as proposed by Head (1974c), but is a distinct type of ejecta. The Cordillera scarp is draped by ejecta, either of the Hevelius or of the Montes Rook Formation, over most of its visible extent (figs. 4.4*A–F*); thus, the scarp predates final ejecta deposition and cannot be the product of postcratering collapse as is shown on the hypothetical cross sections by Hartmann and Yale (1968), Head (1974c), and Howard and others (1974).

The coarse, knobby, weakly lineate texture of the Montes Rook Formation indicates a much smaller radial-ejection component than that of the strongly lineate Hevelius. The Montes Rook Formation probably consists of relatively coherent material ejected in relatively low-velocity, high-angle trajectories, possibly in a distinct second pulse of ejecta. Steep late-forming plumes of ejecta are observed inside the main ejecta cone in some experimental craters formed in layered target materials (Oberbeck, 1975, 1977; Andrews, 1977; Piekutowski, 1977). Blocky materials are lifted steeply from the lower, more cohesive layer and dropped onto the crater and onto the ejecta already emplaced by the earlier, larger plume. In this sense, they constitute an "overturned flap" displaying inverted stratigraphy, as on the rims of simple craters (McCauley, 1977); however, the two ejecta types do not form coherent layers on basin rims. A similar relation between two deposits has been mapped at the Ries crater, Germany (see chap. 3), which also formed in a layered target. The moderately to intensely shocked suevite, derived from the crystalline basement, was lofted and then dropped on unshocked Bunte Breccia, derived moments earlier from the overlying sedimentary beds. In both the experimental and natural craters, the earlier material exits at low angles, and the later at higher angles.

Similar phenomena but a different cause were suggested by Murray (1980), who compared the Montes Rook knobs to the coarse hummocks of probable impact melt on the floors of fresh complex craters (figs. 3.2*D*, 3.32–3.35) and suggested that they were flipped upward and slightly outward as the basin or crater floor rebounded sharply during or after the main cratering. These suggestions entail quarrying of the Montes Rook Formation from a deeper crustal layer than the Hevelius Formation, or from the lunar mantle (McCauley, 1977; Scott and others, 1977; Hodges and Wilhelms, 1978).

Scott and others (1977) mapped a massif facies of the Montes Rook Formation in addition to the knobby facies just described. The massifs of Orientale and other basins typically consist of rectilinear to equidimensional blocks, ranging from a few kilometers to as much as 100 km in length (figs. 4.4*B*, *D*, *E*). The smoothness of their surfaces (except at very high resolution) indicates slope steepness. Their backslopes are typically gentler than their inward-facing slopes (fig. 4.4*B*). Heights are estimated to be as much as 6 km above the plains at their base (Head, 1974b; Howard and others, 1974; Moore and others, 1974); this relief is greater than that between the Cordillera ring and the adjacent shelf. Scott and others (1977) considered the massif facies to consist of a stratigraphic ejecta deposit superposed on a structural uplift, as for similar massifs of Imbrium (Carr and others, 1971; Wilhelms and McCauley, 1971). This interpretation is consistent with the photogeologic appearance of fresh massifs and with the stratigraphy of crater rims. The proportions of ejecta and structurally uplifted material remain unknown.

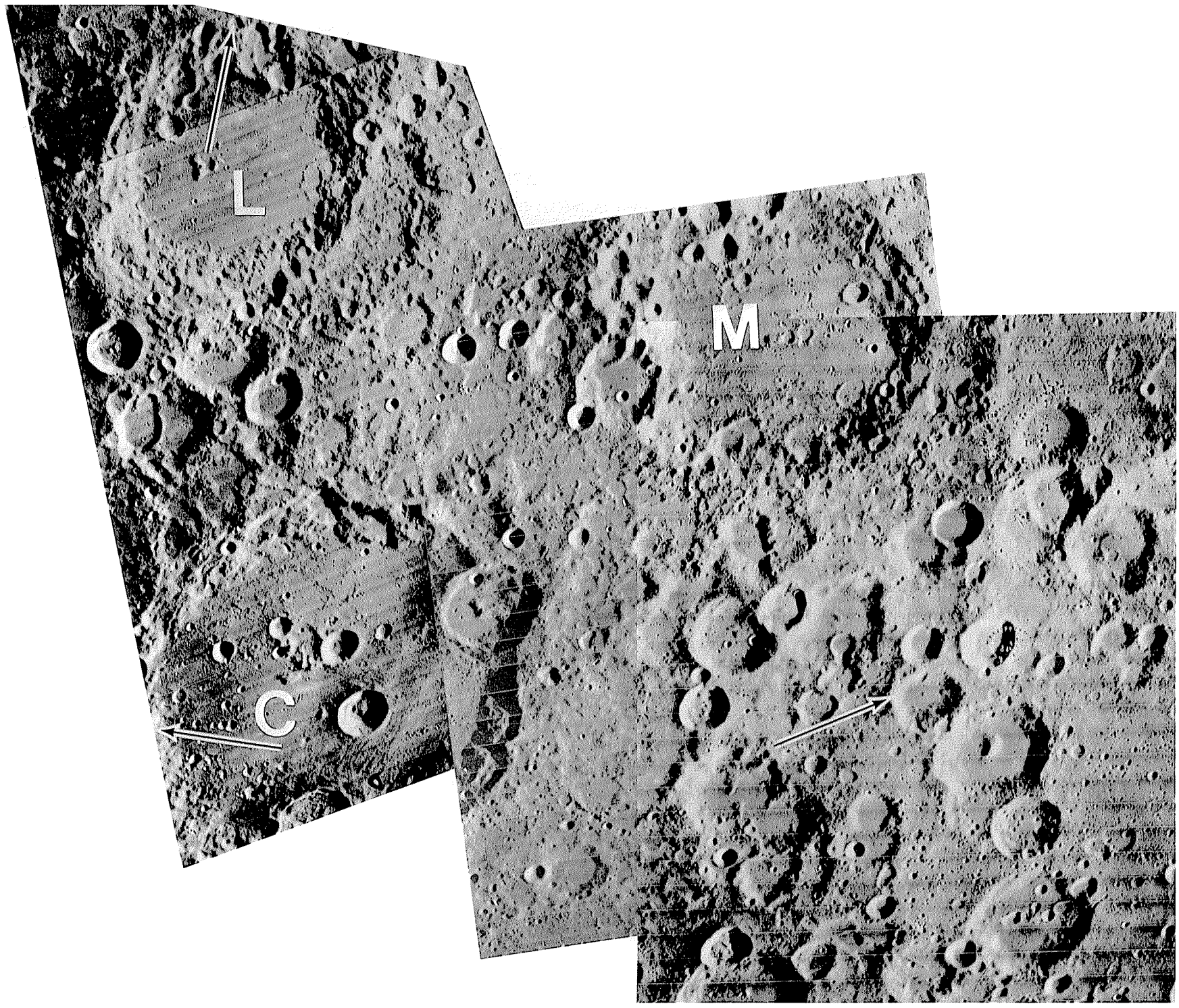

FIGURE 4.6.—South-central terra of nearside, including secondary-impact craters of distant basins.

A. Arrow in crater Clavius (C; 225 km, 48° S., 15°W.) points to Orientale basin, centered 2,000 km to northwest; small sharp craters around arrow are probably secondary to Orientale. Arrow in Longomontanus (L; 145 km, 49.5° S., 22° W.) points to Imbrium basin, centered 2,600 km due north; large overlapping craters around arrow are secondary to Imbrium (Saunders and Wilhelms, 1974). Similar craters on west and north rim of crater Maginus (M; 163 km, 50° S., 6° W.) also are probably secondaries of Imbrium. Right-hand arrow points to Nectaris basin, centered 1,450 km away; three craters above arrow and degraded group below end of shaft are possibly secondary to Nectaris, although lineations are not strictly radial to that basin. Mosaic of Orbiter 4 frames H–119, H–124, and H–136 (right to left).

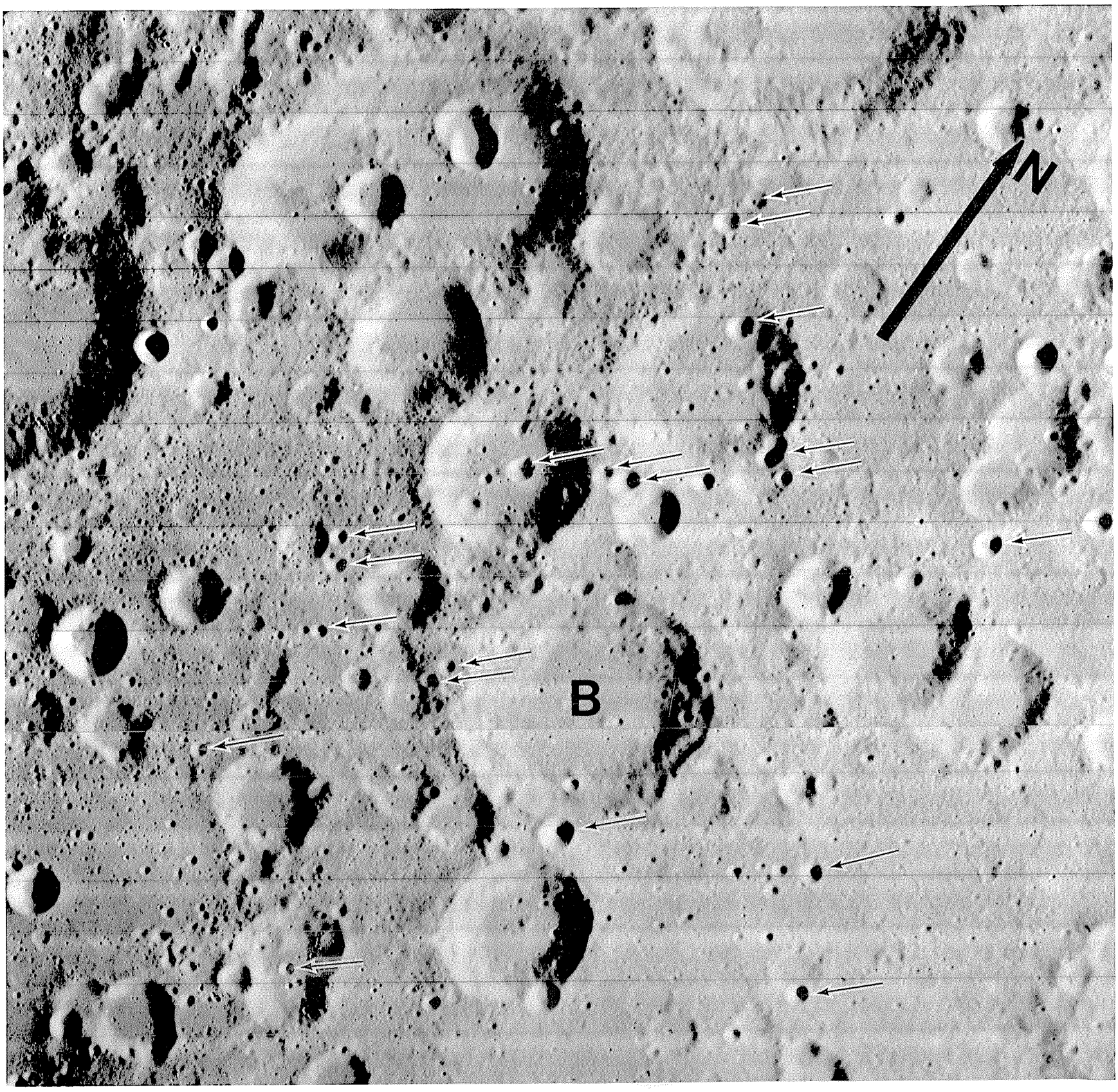

B. Area just east of figure 4.6*A*. Arrows point toward Orientale center and touch fresh-appearing craters that are probable Orientale secondaries. B, crater Baco (70 km, 51° S., 19° E.). Orbiter 4 frame H–100.

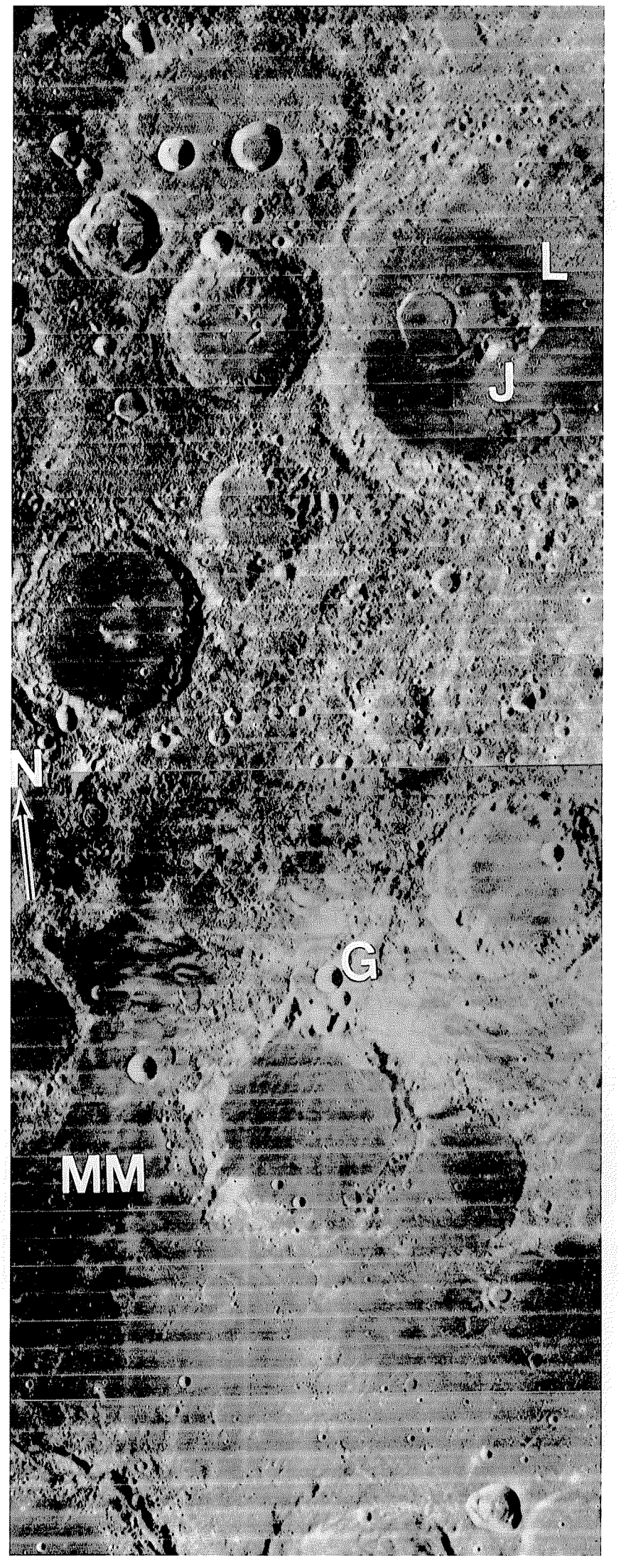

FIGURE 4.7.—Region of Orientale antipode; arrow indicates antipode (20° N., 85° E.). Most of terra is pitted in manner apparently characteristic of antipodes of young basins. MM, Mare Marginis, with bright swirls superposed; G, bright crater Goddard A (12 km), possible source of swirls; J, crater Joliot (143 km); L, mare-flooded fringe of secondary craters of Lomonosov. Mare material in quadrant below and right of Goddard A is among oldest mare units (see chap. 10). Orbiter 4 frame H–17.

Maunder Formation

The Maunder Formation of the Orientale Group is named after the unrelated large impact crater Maunder on the north floor of the central Orientale basin (fig. 4.4*B*). This formation, like others of the Orientale Group, has been described under various names (table 4.3). The Maunder consists of smooth to rolling plains of intermediate albedo, many of which are closely fissured or fractured. As far as observed, the Maunder lies between Mare Orientale and the outer Rook ring and extends the peaks of the inner Rook ring (figs. 4.4*B*, *E*; 4.8).

The fractures are a secondary, superposed property of the unit and thus not a proper part of the definition of a rock-stratigraphic unit (see chap. 7), but they nevertheless characterize it; they led to such descriptions as "corrugated" and "crackly." These fractures are crudely concentric or radial to the basin (fig. 4.4*B*). Most fractures are open, downward-tapering V-shaped gashes, whereas others are larger, flat-floored complex grabens. Many fractures radiate from local centers, and others are aligned along the axes of broad gentle elongate domes, which also characterize the Maunder terrain (fig. 4.4*B*). The fractures are more abundant inside the inner Rook ring than close to the outer Rook ring. Other, larger radial and concentric grabens that are more pervasive probably were formed by later basin subsidence (pl. 5; chap. 6).

Texturally, the Maunder Formation is a scaled-up equivalent of the materials that cover the floors of such fresh unfilled large craters as Tycho and Copernicus (Howard, 1975; Howard and Wilshire, 1975). Though once interpreted as volcanic (Schultz, 1976b, p. 70–77), these floor materials are more convincingly interpreted as impact melts, on the basis of a comparison with terrestrial analogs and stratigraphic analysis (see chap. 3). The thickness of the Orientale melt is difficult

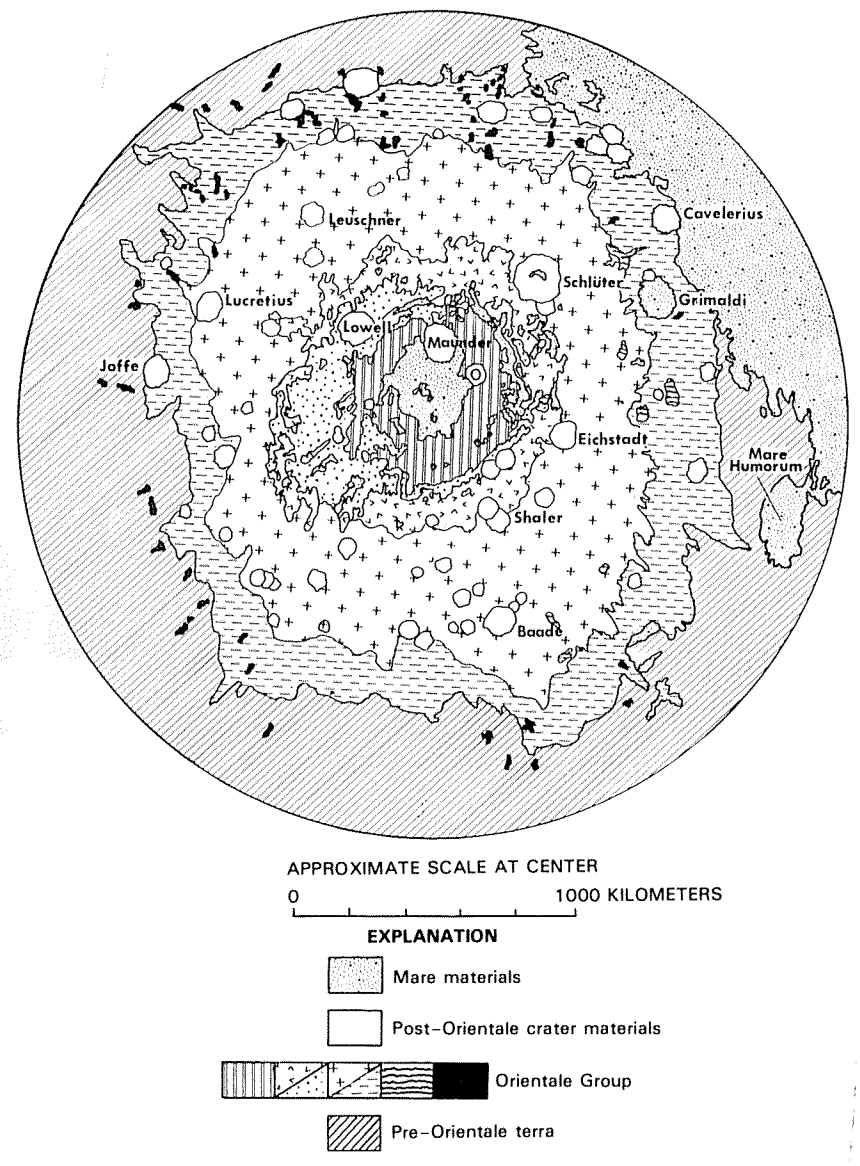

FIGURE 4.8.—Geologic map of Orientale basin, showing major units discussed in this volume. Units of the Orientale Group, from left to right, in "Explanation" are: Maunder Formation (double vertical bars), Montes Rook Formation (check marks, knobby ejecta; dots, massifs), Hevelius Formation (crosses, inner facies; dashes, outer facies), transversely structured parts of the Hevelius Formation (small areas with wavy lines), and some of the many secondary craters (black). From McCauley (1977, fig. 1; see also Scott and others, 1977).

to ascertain; Head (1974c) based an estimate of about 1 km thick on extrapolations from early work on terrestrial craters. The draping and mantling characteristics of much of the Maunder Formation suggest that its material behaved in a fluid manner. Perched shorelines locally visible (fig. 4.4*B*) suggest that it subsided to its present position from some higher topographic level. Sinuous rilles like those of maria (chap. 5) may mark local flowage of the melt (loc. 13, fig. 4.4*B*; Greeley, 1976).

The emplacement of the melt and the formation of the fracture pattern are believed to have been nearly contemporaneous with formation of the elongate ridges and domes, which are more commonly radial or concentric with the basin than equidimensional (fig. 4.4*B*). Mapping of excavations within experimental explosion craters shows that similar structures are compressional anticlines and synclines that formed late in the cratering sequence (Roddy, 1976; McCauley, 1977). If the domes in Orientale also formed late, the Maunder Formation may have been cracked by their uplift. The geometry of the cracks is also consistent with draping on preexisting topography (Head, 1974c), which would be their origin if the folding ended before the melt solidified.

TOPOGRAPHY AND GRAVITY

Favorably illuminated photographs (fig. 1.9) show that the elevations of the concentric troughs of the Orientale basin decrease inward and that Mare Orientale has the lowest surface. The summits of Montes Cordillera and Montes Rook appear to differ less in elevation than do the adjacent troughs. Absolute elevations are less certain because Orientale is not covered by photogrammetric-quality photographs. Preliminary measurements based on Apollo laser altimetry of the basin's north shelf and on profiles obtained from telescopic and Lunar Orbiter photographs suggest that Mare Orientale lies 2.5 to 5.5 km below, and parts of the rings and exterior terrain rise the same distance above, the 1,738-km average radius of lunar terra surfaces (relative to the center of figure) (Howard and others, 1974; Scott and others, 1977; Head and others, 1981; S.S.C. Wu, written commun., 1982). If the mare-basalt fill is less than 1 km thick (Howard and others, 1974), the top of the impact melt in the basin center lies about 3 to 6 km below the 1,738-km datum and about 6 to 11 km below the exterior.

Stairstep structure is also evident in stereoscopic photographs of the more heavily modified Crisium basin, which is a less representative basin but which lay more favorably under the Apollo 15 and 17 ground tracks (fig. 4.9). In the terra rim surrounding Mare Crisium, interring troughs decrease in elevation inward toward the mare. The mountain summits do not decrease in elevation so much (fig. 4.9); that is, the overall relief between a given summit and the adjacent trough increases inward, as it does at Orientale. Absolute elevation differences are also similar—Mare Crisium lies about 4 km below the 1,738-km datum (Sjogren and Wollenhaupt, 1976) and 3 to 6 km below the basin exterior (fig. 4.9). Relative and absolute elevations of another measured basin, Smythii, are remarkably like those of Orientale, despite these basins' substantial difference in relative age (Strain and El-Baz, 1979).

Perturbations of spacecraft orbits have revealed some important features of the Moon's gravity structure. The terrae are gravitationally bland at short wavelengths (see chap. 6; Bills and Ferrari, 1977; Ferrari, 1977). The relatively short-wavelength gravity anomalies with the largest amplitudes are positive, and are called *mascons* (for "mass concentrations"; Muller and Sjogren, 1968). The gravity anomaly of the Orientale interior is positive, but if the basalt of Mare Orientale is removed from the gravity models, a ringlike negative anomaly remains (Scott, 1974; Sjogren and Smith, 1976). The gravity structure of a given basin as a whole requires two bodies—the surficial mare basalt and a raised part of the mantle (fig. 4.10; Wise and Yates, 1970; Phillips and others, 1972; Scott, 1974; Bowin and others, 1975; Sjogren and Smith, 1976). Each basin impact removed an unknown but significant thickness of crustal material (Scott, 1974). The denser mantle then rose to compensate isostatically for the lost mass. On the basis of models for Serenitatis (fig. 4.10), the mantle may be about 20 to 25 km higher under Orientale than in nonbasin regions (Sjogren and Smith, 1976); the same value was found for the Grimaldi basin (Phillips and Dvorak, 1981). The negative anomaly, also found in many basins and fresh craters (Ferrari, 1977; Dvorak and Phillips, 1978), suggests that compensation was incomplete (Sjogren and Smith, 1976). Further alteration of the gravity structure by the later addition of mare basalt resulted in a superisostatic mascon in several basins (see chaps. 5, 6; Baldwin, 1968; Phillips and others, 1972; Scott, 1974; Solomon and Head, 1979, 1980).

Small positive anomalies displayed by Montes Cordillera (Sjogren and Smith, 1976) and Montes Apenninus of the Imbrium basin (Ferrari and others, 1978) indicate (1) a loading of the crust by material removed from the basin and (2) a lithosphere sufficiently strong to support much of this added load.

These gravity models are central to later discussions of basin-excavation depths, mare-basalt localization (chaps. 5, 11, 12), and tectonism (chap. 6). The crust-mantle discontinuity (lunar Moho) probably resembles a series of domelike swells, whose diameter and elevation are approximately proportional to diameters of the overlying basins and which are superposed where basins are superposed. The largest known basin, alternatively called Gargantuan (Cadogan, 1974, 1981) or Procellarum (pl. 3; table 4.2; Whitaker, 1981), presumably overlies the largest mantle uplift and the thinnest crust. This basin was probably responsible for thinning of the crust from the computed average of about 75 km to the observed value of 45 to 60 km under southern Oceanus Procellarum (chap. 1). This thinning had major consequences for later lunar geologic evolution (see chaps. 5, 6, 8–12).

ORIGIN OF RINGS

Introduction

The origin of basin rings has caused considerable interest and controversy because of its importance in impact mechanics and stratigraphy, and because it has proved to be such an obdurate problem (see reviews by Hartmann and Kuiper, 1962; Baldwin, 1963; Mutch, 1970; Hartmann and Wood, 1971; Howard and others, 1974; Moore and others, 1974; Brennan, 1976; Wood and Head, 1976; McCauley, 1977; Wilhelms and others, 1977; Hodges and Wilhelms, 1978; and Croft, 1981). The identity of the boundary of excavation is particularly significant. Discussions of basin-forming mechanics are generally based on knowledge of cratering mechanics derived from small craters, which can be generated experimentally and relatively easily modeled (see chap. 3). Complex craters and large terrestrial astroblemes (1) appear always to have been shallow and not to owe their complex internal structure to the collapse of a deep cavity, (2) contain peaks that seem to have formed by compression of a central zone during subhorizontal centripetal movement, (3) are terraced as a result of this centripetal movement, and (4) are surrounded by deposits and concentrated secondary craters whose extent remains approximately proportional to crater diameter (chap. 3). Some, but not all, of these properties can be extrapolated to basins.

Genetic models

The general increase in complexity with increasing size of impact cavities (figs. 4.2, 4.3, 4.11) has suggested to some investigators that the peaks and terraces of craters and the rings and shelves of basins differ in degree of development because of scale differences. Alternatively, they may have been formed by different processes. Properties of the target material, such as strength and layering, or properties of the impactor, such as impact angle, velocity, size, or shape, may be relatively more important in the larger events. The physical effects of large and small impacts may differ fundamentally in ways that are not yet clear.

A. *Large-basin models.* The main, topographic rim is the boundary of excavation (Baldwin, 1974a; Chao and others, 1975; Oberbeck, 1975; Wilhelms and others, 1977; Hodges and Wilhelms, 1978). Interior rings could have formed in two alternative ways:

1. *Nested craters.* In these models, rings are the rims of subcavities of the main excavation (Oberbeck, 1975; Wilhelms and others, 1977; Hodges and Wilhelms, 1978). Nesting is observed in small craters in the lunar regolith (Oberbeck and Quaide, 1967, 1968; Quaide and Oberbeck, 1968; Oberbeck, 1977), and probably in the Ries (Chao, 1977; Hörz and Ostertag, 1979) and other large terrestrial craters or ringed basins (Phinney and Simonds, 1977; Hodges and Wilhelms, 1978). The initiator of the dual or multiple cavities in experimental and natural terrestrial craters is a discontinuity in the target materials between an overlying weak layer and a less easily cratered substrate. Separate ejecta plumes may be ejected from the nested craters.

2. *Floor uplifts.* Various mechanisms based on cratering mechanics have been proposed. The morphologic similarity between central peaks and rings consisting of peaks (fig. 4.3*B*) suggests that the rings are expanded peaks (Hartmann, 1972a; Baldwin, 1974a; Head, 1974c; McCauley, 1977; Hodges and Wilhelms, 1978). Centripetal movements, akin to those hypothesized for complex craters and observed in large chemical-explosion craters (Jones, 1977; Roddy, 1976, 1977), may form ringlike structures in the innermost basin (McCauley, 1977).

A more violent, oscillatory mechanism akin to that observed in temporary craters formed in liquid has also been suggested. This "tsunami" mechanism, induced by the seismic energy of impact, was first proposed for external rings (Baldwin, 1949, 1972; Van Dorn, 1968, 1969). Baldwin (1974a) then reapplied it to rings of the cavity interior, which is more likely to be fluidized by the intense and sustained shock pressures intrinsic to impacts of large bodies (Baldwin, 1963, p. 163–169; 1974a). Dence and Grieve (1979; Grieve, 1980) recently revived the tsunami mechanism as an explanation for rings, on the basis of the high uplifts of severely weakened subcrater material that they inferred in terrestrial craters; and Murray (1980) independently proposed it on the basis of several photogeologic observations similar to those mentioned in this chapter. The oscillatory model is favored here and is described additionally below (fig. 4.12).

B. *Small-basin models.* An inner ring or the former position of an inner ring marks the boundary of basin excavation.

1. *Late formation.* Passive "megaterracing" is thought to widen the topographic basin by inward movement and rotation of a large annular tract of exterior terrain after excavation has ceased (McCauley, 1968; Mackin, 1969; Hartmann and Yale, 1968; Hartmann and Wood, 1971; Dence and Plant, 1972; Short and Forman, 1972; McGetchin and others, 1973; Gault, 1974; Head, 1974c, 1977; Howard and others, 1974; Moore and others, 1974; Head and others, 1975; Schultz and Gault, 1975a; Croft, 1981). According to this hypothesis, the rear slip surface of the terrace cuts the rim flank outside the excavation boundary and carries that boundary inward. The topographic basin rim is the site of the slip at the rear of the "megaterrace," and the migrated excavation rim becomes an inner ring.

2. *Contemporaneous formation.* A similar geometry results from centripetal movement and rotation during the excavation process

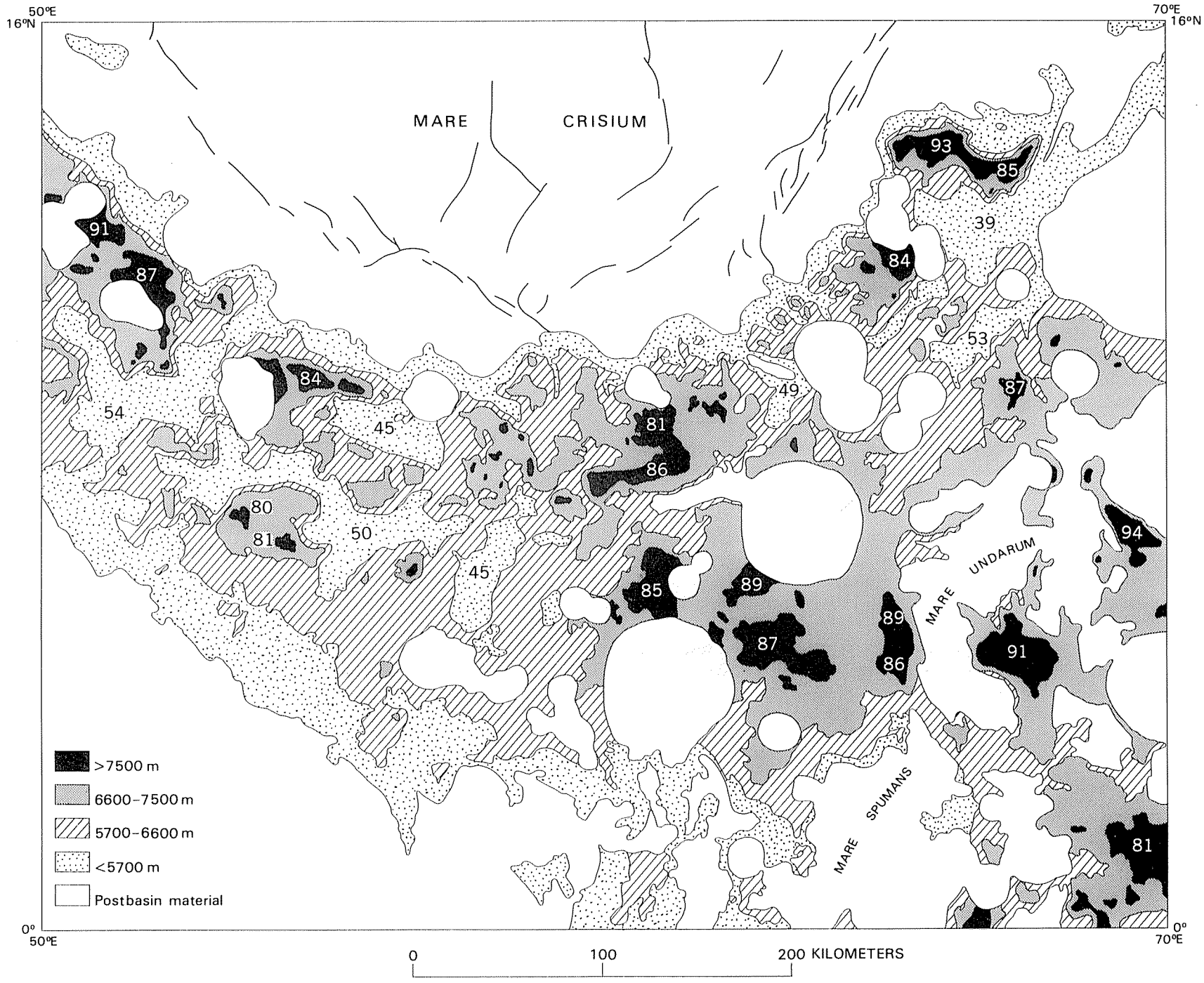

FIGURE 4.9.—Topographic map of southern Crisium basin. Arbitrary vertical datum is 1,730,000 m from Moon's center. Elevations of summits (white numbers on black) and of troughs (black numbers) are shown in hundreds of meters above this datum. Mare Crisium, 3,800 to 3,900 m; Mare Fecunditatis, 5,000 to 5,200 m; Mare Spumans, 5,500 to 5,700 m; Mare Undarum, 6,400 to 6,700 m. Postbasin materials include crater and mare deposits (Olson and Wilhelms, 1974). Topography generalized from LM 62 (1st ed., Sept. 1978), U.S. Defense Mapping Agency.

(McCauley, 1977; Scott and others, 1977). This more active process is observed in large chemical-explosion craters, where centripetal movement opens concentric exterior cracks and depresses an annular shelf between the excavation boundary and the remnant topographic rim. The rim and false rim are overlain by ejecta.

Discussion

1. The topographic rims of such double-ring basins as Schrödinger so closely resemble those of craters in morphology and in their demarcation of the inner boundary of craterlike deposits they must be equivalent in origin (Wilhelms and others, 1977; Hodges and Wilhelms, 1978). That is, the rims approximate the boundary of excavation, except as the excavation cavity was widened by visible craterlike terraces. Thus, the 160-km-diameter inner ring is a feature of the crater interior and not of the boundary of excavation. The inner ring cannot bound the Schrödinger excavation because such a cavity would be smaller than many craters, which have no second ring outside their rims.
2. Similarly, I believe that the topographic rims of larger basins, such as the Cordillera of Orientale, are also the boundaries of excavation. This more controversial conclusion is based on: (a) The abrupt demarcation of the Hevelius Formation at the Cordillera; (b) the elevated massifs along parts of the Cordillera; (c) the absence or ghostlike form[4.1] of prebasin craters inside the Cordillera, in contrast to their abundance outside the Cordillera (Baldwin, 1974a); (d) the rimlike morphology, including steep inner and gentler outer slopes and both scalloped and linear segments (Murray, 1980); (e) the qualitative similarity of both the continuous and discontinuous deposits to crater deposits in overall morphology and zoning; and (f) the proportional extent of the Orientale ejecta in comparison with crater deposits (Wilhelms and others, 1977; Murray, 1980, fig. 7). Montes Cordillera extend as a major well-defined ring around three-fourths of the basin and are not a minor, external structure. Similarly, the 570-km-diameter ring of Hertzsprung and the 600-km-diameter ring of the southern part of Humboldtianum are the boundaries of those excavations (figs. 4.3*O*, *Q*, 4.11; table 4.1). Ejecta extends an average of one basin

[4.1]The presence of ghostlike circular forms inside the Cordillera (Scott and others, 1977) does not obviate the interpretation that the Cordillera is the excavation boundary. If the excavations are shallow, surficial material could be stripped away without destroying the deeper structure of prebasin craters.

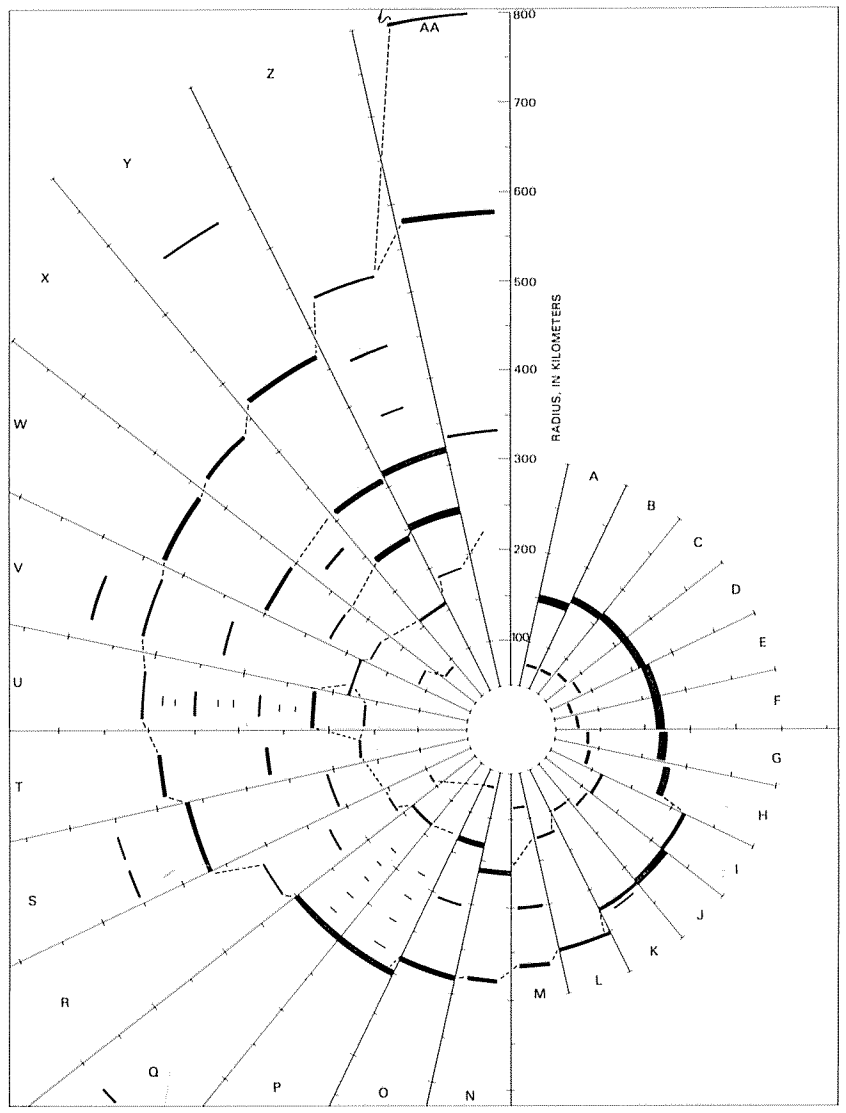

FIGURE 4.11.—Spacing of observed basin rings and ring segments, plotted by radial distance from basin center (after table 4.1, with some approximate additions from pl. 3); see table 4.1 for letter symbols. Length of arc within each sector is approximately proportional to observed circumferential extent of ring; width of line is approximately proportional to prominence. Homologous rings in different basins are connected by dots. Double-ringed structure persists through Korolev (J) or Apollo (L). Innermost and intermediate series begin in Hertzsprung (O) or, possibly, in poorly observed Coulomb-Sarton (M). These new homologous series expand in larger basins through Orientale (Y). Extensive new structure (not completely described here) appears in Crisium (Z) and Imbrium (AA).

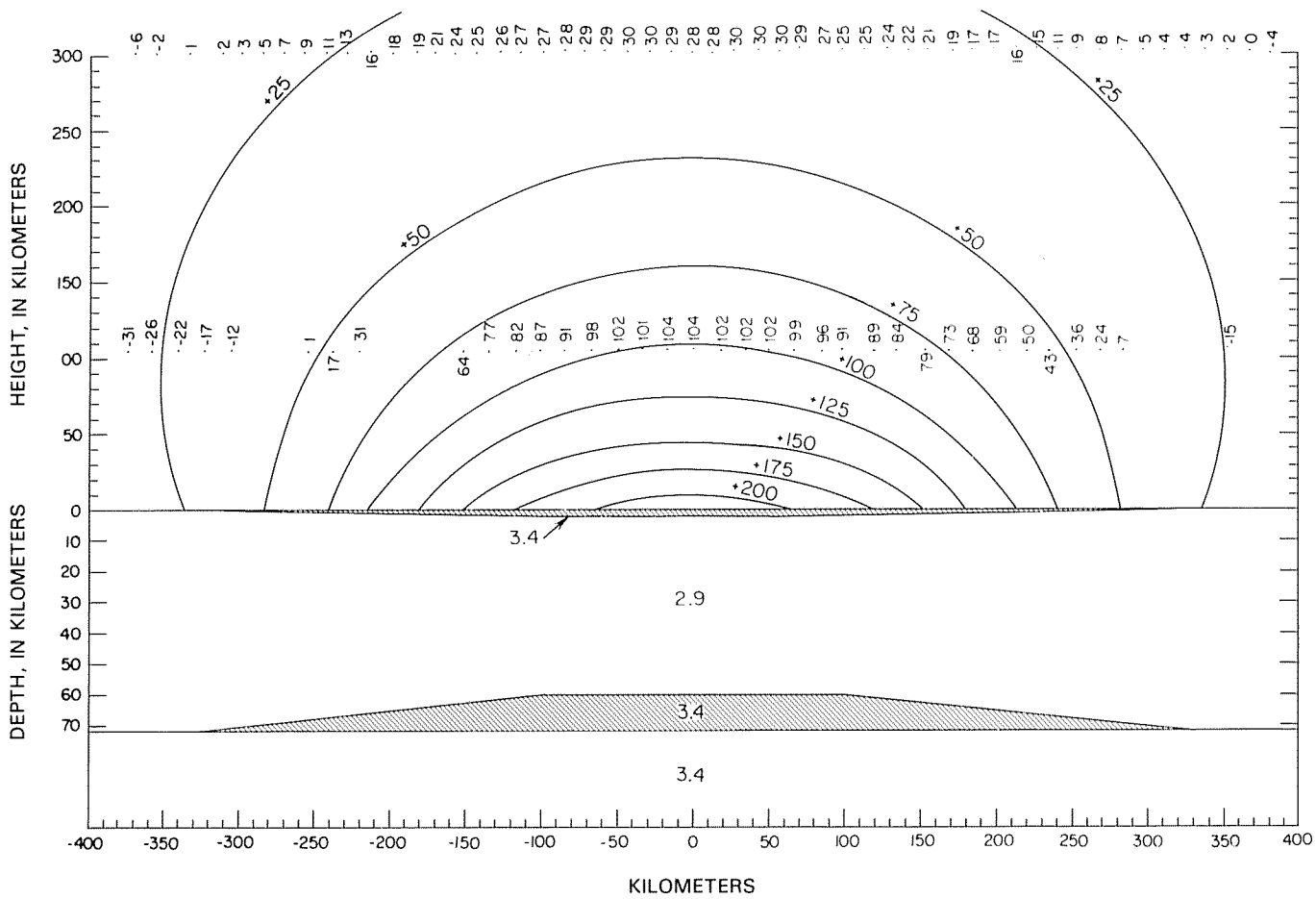

FIGURE 4.10.—Two-body gravity model of Mare Serenitatis (Bowin and others, 1975). A thin plate on surface (mare material) and a mantle uplift each have densities of 3.4 g/cm³ (shaded); terra-crustal density, 2.9 g/cm³. Values in space above mare are observed free-air anomalies from two spacecraft orbits (in milligals); curved lines are isoanomalies of computed free-air gravity.

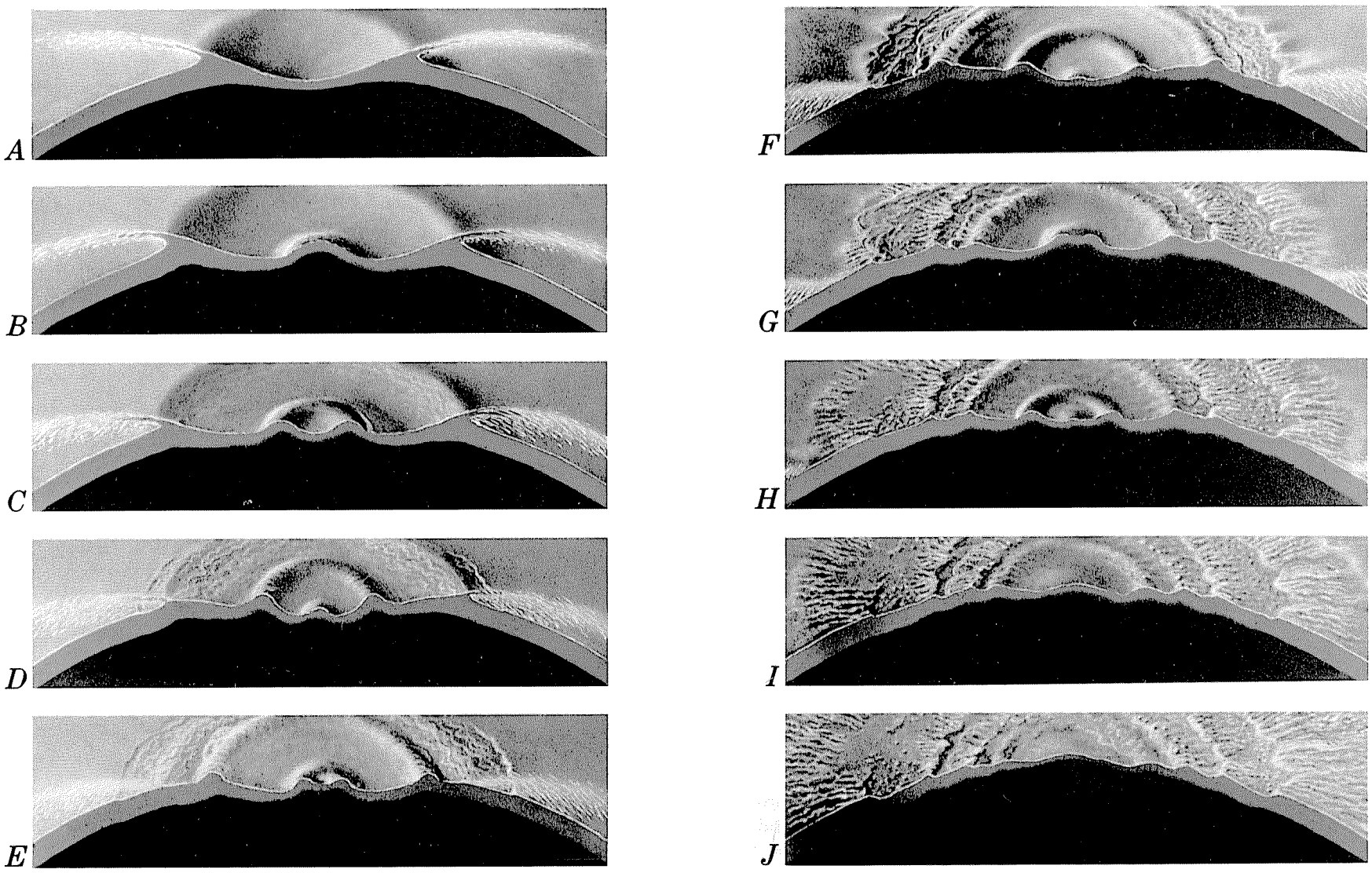

FIGURE 4.12.—Model of basin formation favored here. Drawing by Donald E. Davis, courtesy of the artist.

A. Early stages of growth, resembling simple crater. Target rock is greatly weakened by shock wave.

B. Cavity grows and becomes shallower relative to depth, ejection angle decreases, and central uplift begins as in complex crater.

C. Central uplift collapses to form a temporary double-ringed basin.

D. Center rebounds, as in a waterdrop crater.

E. Wavelike motion enlarges inner ring shown in *C* and *D*, new innermost ring forms from central peak in *D*, boundary of excavation becomes lower, and ejecta blankets basin walls and exterior.

F. Excavation boundary reaches final size, and two inner rings and a central uplift have formed.

G. Ejecta continues to move beyond excavation; continued oscillation of interior causes surge of ejecta from intermediate ring and enlarges innermost ring.

H. Exterior deposits are mostly in place, two rings inside excavation boundary have frozen, but innermost ring continues to grow, and center rises once again.

I. Innermost ring has grown to final size, and central uplift relaxes into low broad mound.

J. Final configuration.

diameter from each of these rings, which are also more rimlike than any others in the basin. Although parts of the interior rings (265 km diam in Hertzsprung and 300 km diam in Humboldtianum) are rimlike, these rings cannot bound the excavations because the similar-size rim crests of Bailly (300 km diam) and Schrödinger (320 km diam) are not surrounded by ring systems or such extensive ejecta (Wilhelms and others, 1977; Murray, 1980, p. 273).

3. Continued, passive terracing after the completion of ejecta deposition is precluded by superposition of the Montes Rook Formation on the Cordillera (McCauley, 1977). Ring formation, whatever its cause, must be an active process driven by the cratering flow.
4. Considerable evidence suggests that basins are shallow excavations (fig. 3.20; Head and others, 1975). First, they presumably were never deeper relative to their diameters than were craters. Copernicus, which is exactly 1/10 the diameter of Orientale, now has a *d*/*D* ratio of 1/25. According to the hypothesis presented earlier, fresh craters were not much deeper when formed than they are now (Pike, 1980a). If Orientale's original *d*/*D* ratio was 1/25, its original, transitory depth was 37 km. This value is close to that obtained by adding the estimated present depth of 6–11 km (exterior terrain to top of impact melt) to the crustal thinning implied by the mantle uplift of 20–25 km. (Its present *d*/*D* ratio is between 1/155 and 1/85, a decrease that indicates substantial rebound since basin formation; furthermore, the negative gravity anomaly would be much greater than observed if no rebound had occurred.) Moreover, these ratios apply only to the central basin inside the 320-km-diameter ring; the shelves, which occupy much more area, are several kilometers shallower. That the cavity-wall slopes were gentle during excavation as well is suggested by the massive surface flows of ejecta and the linear, chainlike arrangement of secondary craters close to the rim (fig. 4.4*D*)—both features indicating low-angle ejection. The apparent paucity or absence of mantle material in the returned samples (chap. 8) furthermore suggests that not even the 3,200-km-diameter Procellarum basin was excavated through the 75-km-thick crust—implying an original *d*/*D* ratio of less than 1/43 for this largest lunar basin.
5. The major interior rings (for example, Montes Rook) probably were formed by some form of active floor uplift. In morphology, they resemble central peaks more closely than they do terrace lips. Their gentle outer slopes and steep inner slopes resemble those of crater rim crests, but the jagged massifs and peaks of their most rugged parts more nearly resemble central peaks. The Rook rings resemble the inner, rugged ring of Schrödinger much more closely than they do the Schrödinger rim.
6. Even if rings and central peaks are both formed by uplifts, the uplift process probably differs. Although a transition from craters to basins is commonly stressed, the interior structure of most craters 200 to 300 km in diameter is poorly developed (fig. 4.2), and peaks actually decrease in absolute width in craters larger than about 70 km in diameter (fig. 3.2*E*; Murray, 1980, p. 282). Therefore, central deformation may be less intense in intermediate-size impacts than in typical complex craters and typical basins. This lull suggests different deformational processes (Hale and Head, 1979; Murray, 1980).
7. Ring uplift may occur during a wavelike deformation of the cavity floor, as follows (fig. 4.12). Highly shocked, effectively fluidized material of the cavity rebounds, probably because of general involvement of the whole floor in wavelike motion to compensate for the cavity. A smaller central zone then partly collapses when

gravity exceeds the inertial force and rock strength. If basin growth stops at this point owing to insufficient energy and all motions "freeze," the result is a double-ring basin similar to those as large as Korolev (440 km) in the size series (figs. 4.3, 4.11, 4.12*C*; table 4.1). In larger impacts, the collapsed part again rises in the center, and so on for as many cycles as are consistent with basin size, target strength, subsurface layering, other properties of the target, and, possibly, projectile size and velocity. Apollo, Hertzsprung, and Humboldtianum are large enough to have acquired a partial third ring (fig. 4.12*E*). Orientale has a fourth ring and a central uplift that signals the start of an additional cycle. Material may flow inward from outside the crater to supply the uplift, as is observed in waterdrop experiments. Sublithospheric flow of an early weak, plastic lunar asthenosphere may have enhanced wavelike ring formation (Van Dorn, 1968, 1969; Murray, 1980; McKinnon, 1981). The uplift freezes from the outside in because the inner part is the most highly fluidized. This explanation attractively accounts both for regular structure, like that in waterdrop experiments, and for irregular structure, as would be expected in heterogeneous and fractured rock materials that do not behave entirely like fluids.

8. Terrane outside the excavation is also deformed. Chapter 3 (see subsection entitled "Deformation and Nonballistic Ejection") mentions that craters may consist of two parts whose sizes are controlled by different scaling laws: an inner excavation cavity scaled to gravity, and an outer unexcavated but deformed zone scaled to rock strength (Croft, 1981). The deformed zone expands relative to the excavation cavity in proportion to impact energy, and thus may be very large for basins. External deformation, which in my model forms fewer rings than is believed by most investigators, has apparently formed arches concentric with the topographic basin rims of Humboldtianum, Orientale, and possibly other basins (pl. 3; table 4.1). Experimental analogs show how these external arches may have formed. Mounds and concentric rings were uplifted around experimental craters created by certain combinations of depth of burst and layering (Piekutowski, 1977), as well as around some large chemical-explosion craters (Baldwin, 1963, p. 122). Seismic energy is transmitted outside the cavity by elastic waves after the shock wave decays (Gault, 1974; Schultz and Gault, 1975a). The elastic waves are refracted and reflected by discontinuities between material layers (Rinehart, 1975; Cooper and Sauer, 1977) and might propagate quite far under favorable circumstances (McKinnon, 1981). Major topographic features, however, are unlikely to have formed by such exterior processes. Although several large rises and troughs in the Sinus Medii region have been interpreted as external anticlines and synclines of Imbrium (Baldwin, 1963, p. 322; Wilhelms, 1964), mapping of the Procellarum basin suggests, instead, that these and many other rings are part of that giant three-ring basin (pl. 3; Whitaker, 1981).
9. The topographic rim, which bounds the ejection, is commonly irregular in large basins. For example, Montes Caucasus east of Mare Imbrium appear to split into two distinct arcs, one continuing northwestward as Montes Alpes and the other continuing northeastward as the north shore of Mare Frigoris (fig. 4.3*AA*). Like the Rook ring of Orientale, the Alpes are the inner bound of knobby ejecta of Imbrium (Alpes Formation; see chap. 10). Like the Cordillera rim of Orientale, the northern Caucasus and the Frigoris shore are the inner bound of radial secondary chains and surface-flow ejecta. The Imbrium rings may have split in the middle of Montes Caucasus because the deformation and excavation were blocked by the preexisting Serenitatis massifs in the south but were freer to expand in the north (Spudis and Head, 1977) into a trough of the Procellarum basin (pl. 3). Spalling, as observed ahead of ejection in some explosion craters (Cooper, 1977, p. 40; Knowles and Brode, 1977, p. 893; Kreyenhagen and Schuster, 1977, p. 989; Maxwell, 1977, p. 1004; Piekutowski, 1977, p. 85–88), may soften up parts of the surrounding terrain for later ejection (Cintala and others, 1978, p. 3805). Ejection from the outer shelves occurred at very shallow angles, more like a surficial stripping than the conical plumes of simple craters.

Conclusions

The clear division of basin structure into rings may have been overemphasized, considering the pattern of hills, peaks, and ridges that lack evident ring structure in several sectors of Hertzsprung, Humboldtianum, Humorum, Nectaris, Serenitatis, western Orientale, Crisium, and Imbrium (fig. 4.3). Partly regular and partly random processes of floor uplift seem to be required to explain this combination of ringlike and irregular patterns. The mechanism favored here is oscillatory uplift of the cavity floor.

The conjecture about ring origin presented here has advanced some ideas as partial explanations that have previously been proposed as total explanations. Terracing has slightly widened the rim of Schrödinger and larger rims, such as the west rim of Korolev (fig. 4.3*J*), but decreases in magnitude with basin size, rather than increasing as predicted by megaterrace models (Murray, 1980, p. 272). In the largest basins, terracing creates only minor slump slivers, such as those northwest of Montes Apenninus (fig. 10.7; Wilhelms and others, 1977; Wilhelms, 1980). The crust-mantle interface or other layering may modulate more basic processes by enhancing ejection, ring uplift, and external deformation. Such oddities as Antoniadi and Compton (figs. 4.2*A*, *B*) must have been caused by some such local effects as layering (Hodges and Wilhelms, 1978). Oscillatory uplift may account both for regularities where enhanced and for irregularities where resisted by rock properties. Knobby ejecta of the interior and near-rim exterior may be flipped out by the oscillation. Oblique impacts probably produced asymmetric ejecta distributions (table 4.4) and may have caused internal asymmetries by distributing coupled energy unevenly, because they release their energy not at a point but along an elongate sloping zone (Gault and Wedekind, 1978). A double or triple impact excavated the Humboldtianum basin (Lucchitta, 1978), and other multiple impacts probably caused the elongation of Moscoviense and Serenitatis. External deformation did occur but created only second-order features, not the main topographic rim or other major arcs and troughs. The topographic rim is the boundary of the excavation cavity but is irregular in many large basins. In conclusion, basins are highly complex natural systems whose origin cannot be learned by straightforward extrapolation from simple cratering mechanics.

SUMMARY OF BASIN-MATERIAL ORIGINS

Orientale and similar, older basins and their deposits were formed in the following sequence of events. (1) A relatively deep, craterlike cavity developed upon impact of a large cosmic projectile; (2) this cavity expanded laterally and ejected massive amounts of material at low angles, forming gouges and thick lineate deposits; (3) the interior rebounded and ejected blocky melt-rich ejecta at higher angles and lower velocities; (4) the rebound collapsed, then oscillated further, each time to successively smaller radii, and left a ring at each hingeline; (5) the last oscillation left a central uplift (known only in Orientale). Ejecta was deposited and secondary craters were formed during events 3 through 5; then, (6) impact melt settled into place, and (7) distant secondary craters were formed.

The interpretations of the well-exposed, well-photographed Orientale deposits presented in this chapter are the principal foundation for interpreting older terra materials. Deposits of 17 basins and the 262-km-diameter transitional feature Milne (fig. 4.2*J*) are mapped here (pl. 3; table 4.1). The presence of rings establishes the existence of 11 basins whose deposits are not identified but which presumably are present; 17 other basins are also mapped whose existence can be disputed (table 4.2). Topographic textures indicative of primary and secondary ejecta emplacement are the first to become blurred over time. The larger secondary craters survive longer but eventually are also obliterated or can no longer be traced to their source basin. Even the mountainous rings may be so thickly buried or heavily pitted by later cratering that they become unrecognizable. Probably, therefore, fewer basins are tabulated (tables 4.1, 4.2) and illustrated here than were actually formed.

Deposits outside the topographic basin rim grade from thick to thin. When fresh, the deposits closest to the rim were coarsely textured, as is the inner facies of the Hevelius Formation at Orientale. These materials probably consist mostly of primary ejecta from the basin. At an average distance of one basin radius, secondary craters begin to dominate the scene. Secondary craters are visible around many basins whose textured ejecta deposits are invisible (see chaps.

8, 9). The inner and outer zones are here mapped separately only where their approximate transition can best be distinguished, around the Orientale, Imbrium, and Nectaris basins (pl. 3). The outer zone is dominated by secondary ejecta derived from local terrain, but the radius where the balance shifts is uncertain. The outer deposits persist for two radii on the average but thin gradually to apparent disappearance. Distinctive grooves at the basin antipodes may indicate a Moon-wide influence of large basins. Much of the barely discernible fine-scale relief of the lunar terrae must have originated by basin ejecta deposition and secondary cratering.

Deposits of both the primary and the secondary zones are lobate and asymmetric. Salients and raylike stringers of secondary craters persist outward for several basin radii in some sectors. "Bow tie" patterns suggesting oblique impacts at low angles are particularly common (pl. 3; table 4.4). Although irregularities are not so evident around old basins, they are inferrable. Therefore, the presence at a given point of the deposits of a given basin cannot be predicted, unless diagnostic textures or mantling relations are visible. Thicknesses are very uncertain.

Several types of deposits are seen only in Orientale or a few other young large basins (table 4.3). Abundant plains mark the transition from the primary to the secondary ejecta of Orientale, Imbrium, and Nectaris but are inconspicuous around smaller or older basins. The presence of degraded older plains is, nevertheless, highly probable in these positions. Planar and fissured impact melt is visible in Orientale (Maunder Formation), but in no other basin with equal certainty. At the large young basins, the presence of the knobby ejecta (Montes Rook and Alpes Formations) inside the basin, on the topographic rim, and on the earlier, thicker deposit (Hevelius Formation and the Fra Mauro Formation around Imbrium) suggests late-stage ejection during floor rebound.

Despite the incompleteness of the lunar record and the shortcomings of the data, a history of lunar basin deposits can be pieced together from superpositional relations, superposed crater densities, and degree of morphologic degradation relative to Orientale. This history constitutes most of the history of the lunar terrae. Chapters 7 through 10 show how knowledge of the mechanisms that emplaced the Orientale deposits supports the interpretations and dating of the older deposits. Breccia and impact-melted rock ascribable to impact processes (chap. 3) were recovered from basin deposits by all the terra-sampling missions (pl. 3; fig. 4.13). Apollo 14 returned melt-bearing ejecta of Imbrium corresponding to the Hevelius Formation (chap. 10), Apollo 15 sampled massifs of Imbrium (chap. 10). Apollo 17 sampled melt-rich materials from the massifs of the Serenitatis basin (chap. 9). Apollo 16 recovered materials of circum-Imbrium plains and hilly-and-furrowed materials that are analogous to Orientale deposits but whose origin is controversial (chaps. 9, 10).

TABLE 4.4.—*Basin asymmetries suggestive of impact angle*

[Azimuths measured clockwise from north. Basins grouped into four age categories (see tables 4.1, 9.3)]

Basin	Center (lat, long)	Azimuths of ejecta lobes	Azimuths of central-basin elongation	Interpreted impact angle
Orientale-------	20° S., 95° W.	150°-240°-330°	---	From 60°.
Schrodinger-----	75° S., 134° E.	150°-330°	---	From 60° or 240°.
Imbrium---------	38° N., 19° W.	160°	Sector 140° elevated	From 70° or 250° (320°-340°?).
Hertzsprung-----	2° N., 129° W.	0°-180°	---	From 90°.
Crisium---------	18° N., 59° E.	0°-80°(?)-155°	80°-260°	From 260°.
Humorum---------	24° S., 40° W.	160°	Sector 160° elevated	From 70°, 250°, or 340°.
Humboldtianum---	61° N., 84° E.	0°-155°	10°-190°	From 260°.
Korolev---------	5° S., 157° W.	10°	---	From 100°.
Moscoviense-----	26° N., 147° E.	10°	30°-210°	From 100°.
Nectaris--------	16° S., 34° E.	145°	---	From 55° or 235°.
Apollo----------	36° S., 151° W.	200°-330°	---	From 85°.
Freundlich-Sharonov.	19° N., 175° E.	0°-210°	---	From 105° or 285°.

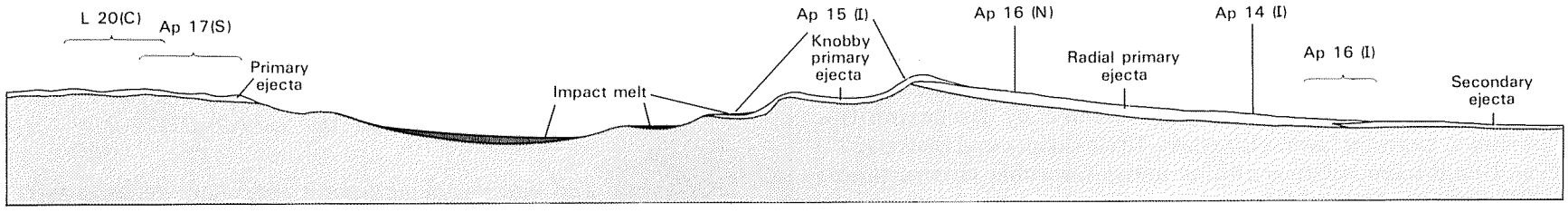

FIGURE 4.13.—Schematic geologic section of typical lunar basin (based on Orientale), showing locations of Apollo (Ap) and Luna (L) sampling sites relative to basin facies sampled (C, Crisium; I, Imbrium; N, Nectaris; S, Serenitatis). Brackets indicate uncertain positions; alternatives are given for Apollo 16, depending on the basin it sampled (see chaps. 9, 10). Right side is based on figure 4.4, left side on figure 4.5. Vertical exaggeration, ×20.